NASA TECHNICAL NOTE

NASA TN D-6733

EFFECT OF LIMITED AMPLITUDE AND RATE OF FLAP MOTION ON VANE-CONTROLLED GUST-ALLEVIATION SYSTEM

by L. Keith Barker, Daniel J. Crawford, and Gene W. Sparrow

Langley Research Center
Hampton, Va. 23365

NATIONAL AERONAUTICS AND SPACE ADMINISTRATION • WASHINGTON, D. C. • MARCH 1972

1. Report No.	2. Government Accession No.	3. Recipient's Catalog No.
NASA TN D-6733		

4. Title and Subtitle	5. Report Date
EFFECT OF LIMITED AMPLITUDE AND RATE OF FLAP MOTION ON VANE-CONTROLLED GUST-ALLEVIATION SYSTEM	March 1972
	6. Performing Organization Code

7. Author(s)	8. Performing Organization Report No.
L. Keith Barker, Daniel J. Crawford, and Gene W. Sparrow	L-8027
	10. Work Unit No.
9. Performing Organization Name and Address	136-62-02-02
NASA Langley Research Center Hampton, Va. 23365	11. Contract or Grant No.
	13. Type of Report and Period Covered
12. Sponsoring Agency Name and Address	Technical Note
National Aeronautics and Space Administration Washington, D.C. 20546	14. Sponsoring Agency Code

15. Supplementary Notes

16. Abstract

An airplane (light transport type) is assumed to be in level flight (no pitching) through atmospheric turbulence which has a mean-square vertical gust intensity of 9.3 $(m/sec)^2$. The power spectral density of the vertical acceleration due to gusts is examined with and without a gust-alleviation system in operation. The gust-alleviation system consisted of wing flaps that were used in conjunction with a vane mounted ahead of the airplane to sense the vertical gust velocity.

The primary purpose of this study was to examine the change in the effectiveness of the gust-alleviation system when the flap motion is limited in amplitude and rate. The alleviation system was very effective if no restrictions were placed on flap motion (rate and amplitude). Restricting the flap amplitude to 0.5 radian did not appreciably change the effectiveness. However, restricting the flap rate did reduce the gust alleviation, and restricting the flap rate to 0.25 rad/sec actually caused the alleviation system to increase the vertical acceleration above that for the no-alleviation situation. Based upon this analysis, rate limiting appears to be rather significant in gust-alleviation systems designed for passenger comfort.

17. Key Words (Suggested by Author(s))	18. Distribution Statement
Limited flap motion Gust-alleviation system Vane sensor	Unclassified – Unlimited

19. Security Classif. (of this report)	20. Security Classif. (of this page)	21. No. of Pages	22. Price*
Unclassified	Unclassified	43	$3.00

*For sale by the National Technical Information Service, Springfield, Virginia 22151

EFFECT OF LIMITED AMPLITUDE AND RATE OF FLAP MOTION ON VANE-CONTROLLED GUST-ALLEVIATION SYSTEM

By L. Keith Barker, Daniel J. Crawford,
and Gene W. Sparrow
Langley Research Center

SUMMARY

An airplane (light transport type) is assumed to be in level flight (no pitching) through atmospheric turbulence which has a mean-square vertical gust intensity of 9.3 $(m/sec)^2$. The power spectral density of the vertical acceleration due to gusts is examined with and without a gust-alleviation system in operation. The gust-alleviation system consisted of wing flaps that were used in conjunction with a vane mounted ahead of the airplane to sense the vertical gust velocity.

The primary purpose of this study was to examine the change in the effectiveness of the gust-alleviation system when the flap motion is limited in amplitude and rate. The alleviation system was very effective if no restrictions were placed on flap motion (rate and amplitude). Restricting the flap amplitude to 0.5 radian did not appreciably change the effectiveness. However, restricting the flap rate did reduce the gust alleviation, and restricting the flap rate to 0.25 rad/sec actually caused the alleviation system to increase the vertical acceleration above that for the no-alleviation situation. Based upon this analysis, rate limiting appears to be rather significant in gust-alleviation systems designed for passenger comfort.

INTRODUCTION

An airplane flying in turbulent air is sometimes subject to motions which cause pilot and passenger discomfort or sickness. For this reason, studies have been made of the use of gust-alleviation systems. The basis of one such system involves using a vane mounted ahead of the aircraft as a gust sensor, and deflecting various airplane control surfaces in response to the vane motion in order to generate forces to counteract gust forces. Theoretical studies have indicated that such a system can be very effective in reducing the aircraft motion in gusty air. However, such studies generally have placed no limit on the amplitude or rate of control-surface motion. (See refs. 1 to 5, for example.) Since practical systems would have some limit on amplitude and rate of motion, it is of interest to determine how such alleviation systems are affected by these limitations.

The present analytical study, therefore, was made to examine the effects of such limitations. In order to simplify the analysis, the airplane was restricted to vertical translation (no pitching). A signal from the gust-sensing vane is used to move the flaps either upward or downward through a linear servomechanism to counteract the effects of the gusts. The effectiveness of the gust-alleviation system is evaluated by examining the power spectral density of the vertical acceleration of the aircraft. The study was restricted to one-dimensional gusts (that is, no spanwise variation of gust intensity) since spanwise variations were found to have little effect unless the wing span becomes comparable with the scale of turbulence (30 meters or more). (See ref. 4.)

SYMBOLS

C_Z vertical-force coefficient

$C_{Z_\alpha} = \frac{\partial C_Z}{\partial \alpha}$, per radian

$C_{Z_{\delta_f}} = \frac{\partial C_Z}{\partial \delta_f}$, per radian

E servosystem input signal, rad

f vertical gust frequency, Hz

g acceleration due to gravity, m/sec^2

K scalar gain constant in flap servosystem

K_2 gain constant in gust spectral shaping filter

L scale of turbulence, m

m mass of airplane, kg

S wing area, m^2

t time, sec

V forward-flight velocity, m/sec

w_g vertical gust velocity (positive upward), m/sec

$\overline{w_g^2}$ mean-square vertical gust velocity, $(m/sec)^2$

z	vertical displacement (positive downward), m
α	angle of attack on wing, rad
$\Delta\alpha$	change in angle of attack on wing from trim condition, rad
α_g	angle of attack on wing due to vertical gust velocity, rad
α_v	total angle of attack of vane, rad
δ_f	flap deflection, rad
$(\delta_f)_L$	limit on flap deflection, rad
$(\dot{\delta}_f)_L$	limit on flap rate, rad/sec
ζ	damping ratio in flap servosystem
$\hat{\mu}_{NS}$	mean estimator of filtered white noise
ρ	air density, kg/m^3
$\hat{\sigma}_{NS}$	standard-deviation estimator of filtered white noise
τ	time required for gust to travel from vane to wing, sec
ϕ_{wg}	one-sided power spectral density of vertical gust velocity, $(m/sec^2)^2/Hz$
$\phi_{\ddot{z}}$	one-sided power spectral density of vertical acceleration of aircraft, $(m/sec^2)^2/Hz$
ω	vertical gust frequency, rad/sec
ω_n	natural frequency of flap servosystem, rad/sec

Primes denote derivatives with respect to distance. Dots over symbols denote derivatives with respect to time. Tildes denote functions of distance.

ANALYSIS

The airplane motion is one-dimensional (translation in z-direction, no pitching). A vane is mounted ahead of the airplane to sense the vertical gust velocity. The vane measurement is then used to deflect the flaps either upward or downward in order to counteract the gusts and reduce the vertical motions of the airplane.

The power spectral density of the vertical acceleration of the airplane is computed and is used to examine the effectiveness of the gust-alleviation system. With no restrictions on flap motion, the equations used are linear and a closed-form expression can be obtained to relate the power spectral density of the aircraft response to the power spectral density of the gust. However, when velocity and/or displacement limits are specified for flap motion, the equations become nonlinear and the power spectral density of the aircraft response must be estimated from the computed time history of the aircraft response to the random gust. Such time histories were generated by an analog computer and, subsequently, analyzed by a digital spectral analysis procedure.

Equation of Motion

The equation of motion used in this study for an aircraft free to move only in the vertical direction is given by

$$m\ddot{z}(t) = \frac{\rho V^2 S}{2}\left[C_{Z_\alpha}\Delta\alpha(t) + C_{Z_{\delta_f}}\delta_f(t)\right] \tag{1}$$

where $\Delta\alpha(t)$ is defined by

$$\Delta\alpha(t) = \frac{\dot{z}(t)}{V} + \alpha_g(t - \tau) = \frac{\dot{z}(t)}{V} + \frac{w_g(t - \tau)}{V} \tag{2}$$

Here $w_g(t - \tau)$ is the vertical gust velocity which hit the vane τ seconds ago and is presently acting on the wing. Hence, equation (1) can be written as

$$m\ddot{z}(t) = \frac{\rho V^2 S}{2}\left\langle C_{Z_\alpha}\left[\frac{\dot{z}(t)}{V} + \frac{w_g(t - \tau)}{V}\right] + C_{Z_{\delta_f}}\delta_f(t)\right\rangle \tag{3}$$

This equation can also be written as

$$\ddot{z}(t) + a_1\dot{z}(t) = -a_1 w_g(t - \tau) + a_2\delta_f(t) \tag{4}$$

where

$$a_1 = -\rho\frac{SV}{2m}C_{Z_\alpha} \tag{5}$$

and

$$a_2 = \rho\frac{SV^2}{2m}C_{Z_{\delta_f}} \tag{6}$$

It is assumed that the flap servomechanism can be described by a second-order differential equation. (See ref. 2.)

$$\ddot{\delta}_f(t) + 2\zeta\omega_n\dot{\delta}_f(t) + \omega_n^2\delta_f(t) = -K\omega_n^2E(t) \tag{7}$$

Two reasonable servosystem inputs are

$$E(t) = \alpha_v(t) = \frac{w_g(t)}{V} + \frac{\dot{z}(t)}{V} \tag{8}$$

and

$$E(t) = \alpha_g(t) = \frac{w_g(t)}{V} = \alpha_v(t) - \frac{\dot{z}(t)}{V} \tag{9}$$

Use of equation (8) means that the flap is moved in response to the total deflection of the vane from its trim position. Use of equation (9) means that the flap moves in response to the true gust angle of attack (that is, the vane angle corrected for airplane motion). The latter case would be more difficult to mechanize than the former case. A preliminary analysis was made to examine each of the two types of control inputs. (See appendix A.) The results showed that rate limiting of the flap motion had similar effects on the power spectral density of the response of the aircraft to random gusts. Somewhat better alleviation was obtained by using just the gust angle of attack (eq. (8)) for the servo input. This result appears to be caused primarily because of a limit-cycle oscillation of the flap which is induced by the rate limits with the $\dot{z}/V$ feedback of equation (8).

Since the effects of rate limiting appeared to be about the same for both types of servo inputs, and to avoid any possible problems with limit cycling, the remainder of the study was restricted to use of equation (9) for the servo input.

When equation (9) is substituted into equation (7), the result is

$$\ddot{\delta}_f(t) + 2\zeta\omega_n\dot{\delta}_f(t) + \omega_n^2\delta_f(t) = -K\omega_n^2\frac{w_g(t)}{V} \tag{10}$$

The gain constant K used in equation (10) was selected to be

$$K = \frac{C_{Z_\alpha}}{C_{Z_{\delta_f}}} \tag{11}$$

This value corresponds to the optimum value of K when the flaps move in phase with a vane that is mounted on the wing aerodynamic center ($\tau = 0$), and there are no constraints on the flap motion.

If the time variation of the vertical gust velocity $w_g(t)$ is specified, equations (3) or (4) and (10) can be used to compute a time history of the vertical acceleration of the aircraft. From this time history, the power spectral density of the vertical acceleration can be computed.

Generation of Vertical Gust Velocity

As stated previously, placing limits on the flap-motion velocity and amplitude resulted in a set of nonlinear equations of motion for the flap and aircraft response and in turn, meant that the power spectral density of the aircraft motion had to be determined from the computed time histories.

To be representative of atmospheric turbulence, it was required that the time history of the vertical gust velocity be normal with a zero mean. The following power spectral density was assumed:

$$\phi_{w_g}(\omega) = \frac{2L}{V}\overline{w_g^2}\,\frac{1}{1+\left(\frac{\omega L}{2V}\right)^2} = \frac{4a_3\overline{w_g^2}}{1+(a_3\omega)^2} \tag{12}$$

where

$$a_3 = \frac{L}{2V} \tag{13}$$

This power spectral density is based on an approximation of the vertical gust correlation function and closely represents turbulence measurements made in wind tunnels. (See ref. 3.)

The techniques for obtaining turbulence having this power spectral density, for including the time lag τ of equation (4), and for obtaining the power spectral density of the aircraft response are given in appendix B.

Aircraft Characteristics

The aircraft mass, aerodynamics, and flight conditions used in this study correspond to those of the light transport airplane of reference 2 and are as follows:

m, kg	3629
S, m^2	32.42
C_{Z_α}, per radian	-5.30
ρ (sea level), kg/m^3	1.223
$C_{Z_{\delta_f}}$, per radian	-0.80
V, m/sec	67

The two turbulence parameters used in this study are:

L, m	610
$\overline{w_g^2}$, $(m/sec)^2$	9.3

The present study covered the range of parameters shown in the following table:

Flap-motion limits		ω_n, rad/sec	ζ
$\lvert(\delta_f)_L\rvert$, rad	$\lvert(\dot{\delta}_f)_L\rvert$, rad/sec		
∞	∞	10	0.7
0.50	∞	10	↓
.50	0.25	4, 10	
↓	.50	↓	
	1.00		

RESULTS AND DISCUSSION

Most of the results of this study will be in the form of the power spectral density of $\ddot{z}$, that is, $\phi_{\ddot{z}}$, as a function of frequency f for different flap-amplitude limits $\lvert(\delta_f)_L\rvert$ and different flap-rate limits $\lvert(\dot{\delta}_f)_L\rvert$. The power spectral density curves presented in this study can be scaled for a wider range of flight conditions as shown in appendix C.

Basic Configuration With No Alleviation

The simulation power spectral density of the aircraft vertical acceleration is shown as a function of gust frequency in figure 1. This curve differs slightly from the corresponding theoretical curve. Since the power spectral density curves for the nonlinear cases must be obtained by the simulation, the simulation curve of figure 1 is used as the basis against which gust alleviation will be measured.

Effectiveness of Flap With No Limits on Amplitude and Rate of Deflection

The effectiveness of the flap with no limit placed on the amplitude or rate of motion is shown in figure 2. With the gust sensor located at the wing aerodynamic center ($V_T = 0$) or at $V_T = 5.22$ meters ahead of the wing aerodynamic center, the flap can eliminate most of the acceleration due to gusts. The alleviation is slightly better with the sensor ahead of the aerodynamic center since it provides a time difference that allows the flap to move toward its commanded position as the gust moves from the sensor to the flap.

Effectiveness of Flap With Limits on Motion Amplitude

The change in flap effectiveness caused by limiting the amplitude of flap travel is shown in figure 3. It was believed that an amplitude limit of $\lvert(\delta_f)_L\rvert = 0.5$ rad would be practical for most transport type airplanes. Placing this limit on flap amplitude did not

reduce the flap effectiveness in alleviating the gust appreciably for either of the two sensor positions. (Compare figs. 2 and 3.)

Effectiveness of Flap With Limits on Both Amplitude and Rate of Deflection

The change in flap effectiveness caused by limiting the rate of deflection of the flap is shown in figures 4 and 5. The results show that a limiting-rate value of $\left|\left(\dot{\delta}_f\right)_L\right| = 1$ rad/sec does not affect the ability of the flap to provide good gust alleviation. Reducing the rate limit to lower values diminishes the alleviation. With a rate limit of $\left|\left(\dot{\delta}_f\right)_L\right| = 0.25$ rad/sec, the flap actually reinforces the gust (improper phasing), and the power spectral density of the aircraft acceleration is worse than that for the no-alleviation situation. Reducing the natural frequency of the flap system from $\omega_n = 10$ rad/sec to $\omega_n = 4$ rad/sec (compare figs. 4 and 5) reduces the maximum gust alleviation which can be obtained with a rate limit of $\left|\left(\dot{\delta}_f\right)_L\right| = 1$ rad/sec.

The effects of rate limiting are summarized in figure 6. This figure shows the percent reduction in the root mean square of the vertical acceleration $\ddot{z}$ as a function of rate limiting $\left|\left(\dot{\delta}_f\right)_L\right|$, natural frequency ω_n, and sensor position $V\tau$. The effects of the various parameters on the root mean square of $\ddot{z}$ have the same trends as they did on the power spectral density of $\ddot{z}$.

Based upon this analysis, rate limiting appears to be rather significant in gust-alleviation systems designed for passenger comfort (lower frequency range); however, because of the limited nature of the study, further analysis is warranted.

CONCLUDING REMARKS

An airplane (light transport type) is assumed to be in level flight (no pitching) through atmospheric turbulence which has a mean square vertical gust intensity of 9.3 $(\text{m/sec})^2$. The power spectral density of the vertical acceleration due to gusts is examined with and without a gust-alleviation system in operation. The gust-alleviation system consisted of using wing flaps in conjunction with a vane mounted ahead of the airplane to sense the vertical gust velocity.

The primary purpose of this study was to examine the change in the effectiveness of the gust-alleviation system when the flap motion is limited in amplitude and rate. The alleviation system was very effective if no restrictions were placed on flap motion (rate and amplitude). Restricting the flap amplitude to 0.5 radian did not appreciably change the effectiveness. However, restricting the flap rate did reduce the gust alleviation, and restricting the flap rate to 0.25 rad/sec actually caused the alleviation system to increase

the vertical acceleration above that for the no-alleviation situation. Based upon this analysis, rate limiting appears to be rather significant in gust-alleviation systems designed for passenger comfort.

Langley Research Center,
National Aeronautics and Space Administration,
Hampton, Va., February 18, 1972.

APPENDIX A

FLAP SERVOSYSTEM INPUT E(t)

Two expressions were examined for the flap servosystem input; namely,

$$E(t) = \alpha_g(t) = \frac{w_g(t)}{V} = \alpha_V(t) - \frac{\dot{z}(t)}{V} \tag{A1}$$

and

$$E(t) = \alpha_V(t) = \frac{w_g(t)}{V} + \frac{\dot{z}(t)}{V} \tag{A2}$$

Equation (A1) represents the angle of attack on the vane due to the gust; equation (A2) represents the total angle of attack measured by the vane.

For a random time variation of the vertical gust velocity $w_g(t)$, equations (3) or (4) and (7) can be used in conjunction with either equation (A1) or (A2) to generate a time history of the vertical acceleration of the airplane. From this time history, the power spectral density of the vertical acceleration can be computed. The reason for computing the power spectral density directly from the time history is that limits placed on the flap motion cause the equations to become nonlinear so that the usual closed-form expression cannot be used.

The power spectral density of the vertical acceleration $\phi_{\ddot{z}}$ is shown in figure 7 for the two types of input given by equations (A1) and (A2). The natural frequency of the flap servo system was $\omega_n = 4$ rad/sec, and the vane location was $V_T = 5.22$ meters ahead of the wing aerodynamic center. The flap amplitude limit was 0.5 radian. The flap rate limits used were 1 rad/sec, 0.5 rad/sec, or 0.25 rad/sec.

From figure 7 it appears that better gust alleviation is attained by using equation (A1) rather than equation (A2), since the power spectral density curve associated with equation (A1) is generally below the curve associated with equation (A2). As the flap rate limit is made more stringent (lowered), this difference becomes more pronounced. The reason the power spectral density associated with equation (A2) is amplified appears to result from a limit-cycle oscillation of the flaps which is induced by the rate limits with the $\dot{z}/V$ feedback required in using equation (A2). (See fig. 8.)

The following table shows the root-mean-square values of $\ddot{z}$ corresponding to the various power spectral density curves:

Flap rate limit, $\left\|(\dot{\delta}_f)_L\right\|$, rad/sec	Flap amplitude limit, $\left\|(\delta_f)_L\right\|$, rad	Root mean square of $\ddot{z}$ based on –	
		Equation (A2)	Equation (A1)
0.25	0.5	2.1	2.0
.50	↓	1.7	1.4
1.00	↓	1.4	1.3

As expected, the values associated with equation (A2) are larger than those associated with equation (A1).

Although the results appear to be better when the input given by equation (A1) is used, it would appear that equation (A2) would be easier to mechanize. The limit-cycle oscillation might possibly be avoided by using some type of nonlinear flap control law.

APPENDIX B

COMPUTER SIMULATION AND SPECTRAL ANALYSIS PROGRAM

A block diagram of the gust-alleviation system is shown in figure 9. The vertical gust velocity $w_g(t)$ is sensed by the vane. Later (after transport delay), this same gust velocity $w_g(t - \tau)$ hits the wing. The flap, meanwhile, moves in response to the gust presently sensed by the vane $w_g(t)$.

The mathematical models of the flap servo (eq. (10)) and the aircraft (eq. (4)) were implemented on a general-purpose analog computer which was operated in conjunction with a digital computer operating in the real-time mode. The functions of the analog computer were to generate the gust disturbance velocities and to solve the equations of motion of the flap and aircraft. The functions of the digital computer were to provide the transport delay which appears in equation (4) and to calculate the power spectral density of the gust input and aircraft response.

Atmospheric Turbulence Generator

Figure 10 is a block diagram of the vertical gust generator. It consists of a noise source, a spectral shaping filter, and a circuit to insure that w_g has a mean of zero and the desired variance $\overline{w_g^2}$. The noise source was a variable-frequency, constant-variance device which gave a continuous Gaussian signal with a mean-square voltage of 10, with a selected half-power point at 15 Hz. The spectral-shaping filter was a first-order filter with half-power point at about 0.03 Hz (that is, $V/\pi L$). Thus, the spectrum of the noise source, with the half-power point at 15 Hz, was much flatter than the spectrum after the filter and, consequently, had an almost white spectrum with respect to the filter. The static gain of the filter K_2 was somewhat arbitrary because an automatic gain circuit controlled the mean and variance from the desired simulated gust.

Figure 11 shows the method of estimating the mean and standard deviation of the filtered gust signal. The integrators were allowed to operate at least 1000 seconds before being used in the simulation. The purpose was to achieve good statistical estimates of the mean and standard deviation prior to any analysis of the aircraft response. The integrators were not reset for several simulation runs. This estimation technique required the generation of the function t^{-1} for $t \geq 1000$ seconds. This function was implemented with the circuit shown in figure 12.

Aircraft Dynamics

The diagram for simulation of the flap motion is shown in figure 13. Either of the two limits (rate or amplitude) could be selected. The limiter on flap position drives the

flap rate to zero when the flap is at its limits of travel; a conventional velocity limit was used for flap rate. The two limiters acted independently.

The variable time delay was implemented by use of a potentiometer, two analog-to-digital converters, a digital-to-analog converter, and a data buffer in the digital computer. Although the potentiometer could be varied continuously, the corresponding time delay varied in discrete steps of 1.0 sample period (0.03125 second) from a value of 1.5 sample periods (0.046875 second) to a value of 32.5 sample periods (1.015625 seconds). The digital computer was bypassed when simulating the zero-transport-delay condition. The dynamics of the aircraft were simulated as shown in figure 14.

Spectral Density Calculations

The power spectral densities of two quantities were desired: that of the aircraft acceleration (for evaluation of the gust-alleviation system) and that of the gust input (to ascertain that the gust characteristics were shaped as desired). Both quantities were computed in the same manner. The following description of the mechanization of the computer for power spectral density computations is written in general terms.

The one-sided spectrum of a stationary random process $x(t)$ is given by

$$\phi_x(\omega) = 2 \int_{-\infty}^{\infty} \theta_x(\tau)\, e^{-i\omega\tau}\, d\tau \tag{B1}$$

where $\theta_x(\tau)$ is the autocorrelation function of $x(t)$. If $x(t)$ is also ergodic, the autocorrelation function of x is defined by

$$\theta_x(\tau) = \lim_{T\to\infty} \frac{1}{T} \int_0^T x(t)\, x(t - \tau)\, dt \tag{B2}$$

To insure that the integral in equation (B1) is bounded, the autocovariance function $\psi_x(\tau)$ is used instead of the autocorrelation function $\theta_x(\tau)$. If $x(t)$ has a zero mean, these two functions are equivalent. The autocovariance function is defined as

$$\psi_x(\tau) = \theta_x(\tau) - \overline{x^2} \tag{B3}$$

where $\overline{x^2}$ is the mean-square value of $x(t)$. In the present study the autocovariance function was approximated by the summation

$$\psi_x(\tau) = \frac{1}{N - l} \sum_{k=l}^{N} x(k\,\Delta t)\, x(k\,\Delta t - \tau) - \hat{\bar{x}}^2 \tag{B4}$$

where $\hat{\bar{x}}$ is the estimate of the mean value of x, and $\tau = l\,\Delta t$. In the summation, $N + 1$ represents the number of sample points on the time history.

Since the autocorrelation $\phi_x(\omega)$ is an even function,

$$\phi_x(\omega) = 4 \int_0^\infty \psi_x(t) \cos \omega t \, dt \tag{B5}$$

In the present study $\phi_x(\omega)$ was approximated by the summation

$$\phi_x(\omega) = 2 \Delta t \left[\psi_x(0) + 2 \sum_{j=1}^{p-1} \psi_x(j \Delta t) \cos(j \Delta t \omega) + \psi_x(p \Delta t) \cos(p \Delta t \omega) \right] \tag{B6}$$

where

$$\omega = \frac{\pi k}{\Delta t p}$$

and $p + 1$ is the number of points on the power spectral density curve, and the index k is called the harmonic number. This curve was smoothed by using a Hanning filter. (See ref. 6.)

The sample period Δt used in this study was 0.125 second. Approximately 21 minutes of running time T_r was required for each simulated run. This time was determined by the desired variance on the statistical estimates and also by the resolution of the spectral density curves. The criterion used to select the running time is

$$T_r = \frac{1}{\beta_e \epsilon^2} \tag{B7}$$

where

$$\beta_e = \frac{1}{p \Delta t} \tag{B8}$$

and ϵ^2 is a measure of the variation of the estimate and is defined by

$$\epsilon^2 = \frac{\operatorname{var}\left[\hat{\phi}_x(\omega)\right]}{\phi_x{}^2(\omega)} \tag{B9}$$

In the present study, the values used for β_e and ϵ were 0.08 and 0.1, respectively.

When no limits are placed on δ_f and $\dot{\delta}_f$, a closed-form expression can be obtained for the power spectral density of the aircraft acceleration. The expression is

$$\phi_{\ddot{z}}(\omega) = \left[\frac{(a_1 \omega)^2}{\omega^2 + a_1{}^2} \right] \left\{ \frac{\omega_n{}^2}{\omega^4 + 2\omega_n{}^2 \left(2\zeta^2 - 1\right) \omega^2 + \omega_n{}^4} \left[\omega_n{}^2 - 2\left(\omega_n{}^2 - \omega^2\right) \cos \tau\omega \right.\right.$$

$$\left.\left. - 4\zeta\omega_n \omega \sin \tau\omega \right] + 1 \right\} \phi_{w_g}(\omega) \tag{B10}$$

where a_1 is defined by equation (5).

In order to check the accuracy of the computer simulation and the power spectral density computations of the computer, results for $\phi_{\ddot{Z}}(\omega)$ of equation (B10) were compared with those of the computer. The results are shown in figure 15 and show good agreement.

APPENDIX C

APPLICATION OF RESULTS TO WIDER RANGE OF FLIGHT CONDITIONS

The purpose of the following discussion is to present a procedure for interpreting the power spectral density curves of this study for different forward-flight speeds and gust intensities.

Scaling Results for Changes in Forward-Flight Speed

Taylor's hypothesis which assumes the turbulence to be "frozen" in space is often employed in studying the effects of rough air on airplanes. In this manner, the vertical gust velocity is essentially a function of position in space. Let λ be a space parameter so that

$$\lambda = Vt \tag{C1}$$

Equations (3) and (10), written in terms of the distance λ, become

$$m\tilde{z}''(\lambda) = \frac{\rho S}{2}\left\{C_{Z_\alpha}\left[\tilde{z}'(\lambda) + \frac{\tilde{w}_g(\lambda - V\tau)}{V}\right] + C_{Z_{\delta_f}}\tilde{\delta}_f(\lambda)\right\} \tag{C2}$$

and

$$\tilde{\delta}_f''(\lambda) + 2\zeta\Omega_m\tilde{\delta}_f'(\lambda) + \Omega_m{}^2\tilde{\delta}_f(\lambda) = -K\Omega_m{}^2\frac{\tilde{w}_g(\lambda)}{V} \tag{C3}$$

The primes denote differentiation with respect to λ, the tilde signs denote functions of λ, and

$$\Omega_m = \frac{\omega_n}{V} \tag{C4}$$

The limits on the flap amplitude motion in space and time are the same. However, the limit on flap rate must be scaled by the velocity V as

$$\left(\tilde{\delta}_f'\right)_L = \frac{1}{V}\left(\dot{\delta}_f\right)_L \tag{C5}$$

The power spectral density of the space function $\tilde{z}''(\lambda)$ is related to the power spectral density of the time function $\ddot{z}(t)$ by

$$\phi_{\tilde{z}''(\lambda)}(\Omega) = \frac{1}{V^3}\,\phi_{\ddot{z}(t)}(\omega) \tag{C6}$$

where

$$\Omega = \frac{\omega}{V} \tag{C7}$$

Equations (C6) and (C7) are derived in appendix D.

Equations (C2) and (C3) show that if the gust intensity is scaled in space in direct proportion to velocity, then the vertical motion will remain the same when plotted against λ, provided $V\tau$, ζ, and ω_n/V are held constant. This statement also means that the power spectral density $\phi_{\ddot{z}''(\lambda)}(\Omega)$ remains the same when plotted as a function of Ω.

Consider two forward-flight speeds V and $V_1 = CV$ (V is the flight speed used in this study). Figure 16 shows the various relationships which are involved in going from $\phi_{\ddot{z}(t)}(\omega)$ to $\phi_{\ddot{z}''(\lambda)}(\omega)$ and then going from $\phi_{\ddot{z}''(\lambda)}(\omega)$ to $\phi_{\ddot{z},1(t)}(\omega_1)$. The subscript 1 denotes motion corresponding to V_1.

The relations shown in figure 16 can be used to obtain the desired transformation equations between $\phi_{\ddot{z}(t)}(\omega)$ and $\phi_{\ddot{z},1(t)}(\omega_1)$. These equations are

$$\phi_{\ddot{z},1(t)}(\omega_1) = \left(\frac{V_1}{V}\right)^3 \phi_{\ddot{z}}(\omega) = C^3 \phi_{\ddot{z}}(\omega) \tag{C8}$$

$$\left(\delta_{f,1}\right)_L = \frac{V_1}{V}\left(\dot{\delta}_f\right)_L = C\left(\dot{\delta}_f\right)_L \tag{C9}$$

$$\omega_1 = \frac{V_1}{V}\,\omega = C\omega \tag{C10}$$

In brief, assume the gust angle of attack to be a constant space function. Let V change by a constant factor C. If ω_n/V, ζ, and $V\tau$ are held constant and $\left(\dot{\delta}_f\right)_L$ changes by the factor C, then the power spectral density curves of this study apply by simply changing the $\phi_{\ddot{z}(\omega)}(\omega)$ and ω (or f) scales by C^3 and C, respectively.

Scaling Results for Changes in Gust Intensity

The power spectral density curves of this study can also be scaled for different gust intensities while the same forward speed V is kept. Suppose the vertical gust intensity is scaled by a constant factor B. Let the resulting motion be denoted by the subscript 1. Equations (3) and (10) then can be written as

$$m\,\frac{\ddot{z}_1(t)}{B} = \frac{\rho V^2 S}{2}\left\{C_{Z_\alpha}\left[\frac{\dot{z}_1(t)}{B} + \frac{w_g(t-\tau)}{V}\right] + C_{Z_{\delta_f}}\,\frac{\delta_{f,1}(t)}{B}\right\} \tag{C11}$$

and

$$\frac{\ddot{\delta}_{f,1}(t)}{B} + 2\zeta\omega_n\,\frac{\dot{\delta}_{f,1}(t)}{B} + \omega_n^2\,\frac{\delta_{f,1}(t)}{B} = -K\omega_n^2\,\frac{w_g(t)}{V} \tag{C12}$$

Assume that the flap amplitude varies directly by the same factor B as the gust intensity. Thus,

$$\delta_{f,1}(t) = B\delta_f(t) \tag{C13}$$

and

$$\dot{\delta}_{f,1}(t) = B\dot{\delta}_f(t) \tag{C14}$$

By comparing the forms of equations (C11) and (C12) with the forms of equations (3) and (10) under this assumption, it can be seen that

$$B\ddot{z}(t) = \ddot{z}_1(t) \tag{C15}$$

From equation (C15), it then follows that

$$\phi_{\ddot{z},1}(\omega) = B^2\phi_{\ddot{z}}(\omega) \tag{C16}$$

The limits on the flap motion follow from equations (C13) and (C14) as

$$\left(\delta_{f,1}\right)_L = B\left(\delta_f\right)_L \tag{C17}$$

and

$$\left(\dot{\delta}_{f,1}\right)_L = B\left(\dot{\delta}_f\right)_L \tag{C18}$$

The desired transformation equations are equations (C16), (C17), and (C18).

APPENDIX D

DEVELOPMENT OF THEOREM AND APPLICATIONS

Theorem Development

The following theorem, developed in the course of this study, is very useful in relating power spectral density functions when certain conditions exist.

Theorem: Consider two stationary random processes $f(x)$ and $g(y)$, where

$$y = C_1 x \tag{D1}$$

and C_1 is a constant. If the processes are ergodic and

$$f(x) = C_2 g(y) \tag{D2}$$

where C_2 is a constant, then it can be shown that

$$\psi_{f(x)}(\Delta x) = C_2{}^2 \psi_{g(y)}(\Delta y) \tag{D3}$$

where $\psi_{f(x)}(\Delta x)$ and $\psi_{g(y)}(\Delta y)$ are the autocorrelation functions of $f(x)$ and $g(y)$, respectively. Also,

$$\phi_{f(x)}(\omega_x) = \frac{C_2{}^2}{C_1} \phi_{g(y)}(\omega_y) \tag{D4}$$

provided the frequencies ω_x and ω_y are related by

$$\omega_y = \frac{\omega_x}{C_1} \tag{D5}$$

where $\phi_{f(x)}(\omega_x)$ and $\phi_{g(y)}(\omega_y)$ are the power spectral density functions of $f(x)$ and $g(y)$.

Proof: The autocorrelation function for $f(x)$ is defined by

$$\psi_{f(x)}(\Delta x) = \lim_{x \to \infty} \frac{1}{2x} \int_{-x}^{x} f(x)\, f(x + \Delta x)\, dx \tag{D6}$$

Since $f(x) = C_2 g(y)$ and $\Delta y = C_1 \Delta x$,

$$\psi_{f(x)}(\Delta x) = \lim_{y \to \infty} \frac{C_2{}^2}{2y} \int_{-y}^{y} g(y)\, g(y + \Delta y)\, dy = C_2{}^2 \psi_{g(y)}(\Delta y) \tag{D7}$$

The power spectral density of $f(x)$ is defined by

$$\phi_{f(x)}(\omega_x) = \int_{-\infty}^{\infty} \psi_{f(x)}(\Delta x)\, e^{(-i\omega_x \Delta x)}\, d(\Delta x) \tag{D8}$$

Substituting equation (D7) into equation (D8) gives

$$\phi_{f(x)}(\omega_x) = \int_{-\infty}^{\infty} C_2{}^2 \psi_{g(y)}(\Delta y)\, e^{(-i\omega_x \Delta x)}\, d(\Delta x) \tag{D9}$$

Since $\Delta y = C_1 \Delta x$, equation (D9) can be written as

$$\phi_{f(x)}(\omega_x) = \frac{C_2{}^2}{C_1} \int_{-\infty}^{\infty} \psi_{g(y)}(\Delta y)\, e^{(-i\omega_y \Delta y)}\, d(\Delta y) \tag{D10}$$

where

$$\omega_y = \frac{\omega_x}{C_1} \tag{D11}$$

By definition,

$$\phi_{g(y)}(\omega_y) = \int_{-\infty}^{\infty} \psi_{g(y)}(\Delta y)\, e^{(-i\omega_y \Delta y)}\, d(\Delta y) \tag{D12}$$

From equation (D12), it can be seen that equation (D10) can be written as

$$\phi_{f(x)}(\omega_x) = \frac{C_2{}^2}{C_1}\, \phi_{g(y)}(\omega_y) \tag{D13}$$

Applications

As an example in the use of the theorem, let $\ddot{z}(t) = V^2 \tilde{z}''(\lambda)$, where $\lambda = Vt$. In this case, $f(x) = \ddot{z}(t)$, $g(y) = \tilde{z}''(\lambda)$, $C_2 = V^2$, and $C_1 = V$. Let $\omega_x = \omega$ and $\omega_y = \Omega$. By direct substitutions into equations (D4) and (D5), it follows that

$$\phi_{z(t)}(\omega) = V^3 \phi_{\tilde{z}''(\lambda)}(\Omega)$$

where

$$\Omega = \frac{\omega}{V}$$

Another interesting example is the relationship between the power spectral densities of the vertical gust velocity written as a function of space λ and time t. Here

$$w_g(t) = \tilde{w}_g(\lambda)$$

where

$$\lambda = Vt$$

In this case, $f(x) = w_g(t)$, $g(y) = \tilde{w}_g(\lambda)$, $C_1 = V$, and $C_2 = 1$. Let $\omega_x = \omega$ and $\omega_y = \Omega$. Then, application of the theorem shows that

$$\phi_{w_g(t)}(\omega) = \frac{1}{V}\,\phi_{\tilde{w}_g(\lambda)}(\Omega)$$

where

$$\Omega = \frac{\omega}{V}$$

It should be noted that some authors define the power spectral density function in a slightly different manner than that indicated by equation (D8) or (D12). Sometimes a factor of $1/\pi$ or $1/2\pi$ will precede the integral. The results of the theorem, however, still apply in each case.

REFERENCES

1. Phillips, William H.; and Kraft, Christopher C., Jr.: Theoretical Study of Some Methods for Increasing the Smoothness of Flight Through Rough Air. NACA TN 2416, 1951.

2. Boucher, Robert W.; and Kraft, Christopher C., Jr.: Analysis of a Vane-Controlled Gust-Alleviation System. NACA TN 3597, 1956.

3. Diederich, Franklin W.; and Drischler, Joseph A.: Effect of Spanwise Variations in Gust Intensity on the Lift Due to Atmospheric Turbulence. NACA TN 3920, 1957.

4. Barker, L. Keith; and Sparrow, Gene W.: Analysis of Effects of Spanwise Variations of Gust Velocity on a Vane-Controlled Gust-Alleviation System. NASA TN D-6126, 1971.

5. Barker, L. Keith: Effects of Spanwise Variation of Gust Velocity on Alleviation System Designed for Uniform Gust Velocity Across Span. NASA TN D-6346, 1971.

6. Bendat, Julius S.; and Piersol, Allan G.: Measurement and Analysis of Random Data. John Wiley & Sons, Inc., c.1966.

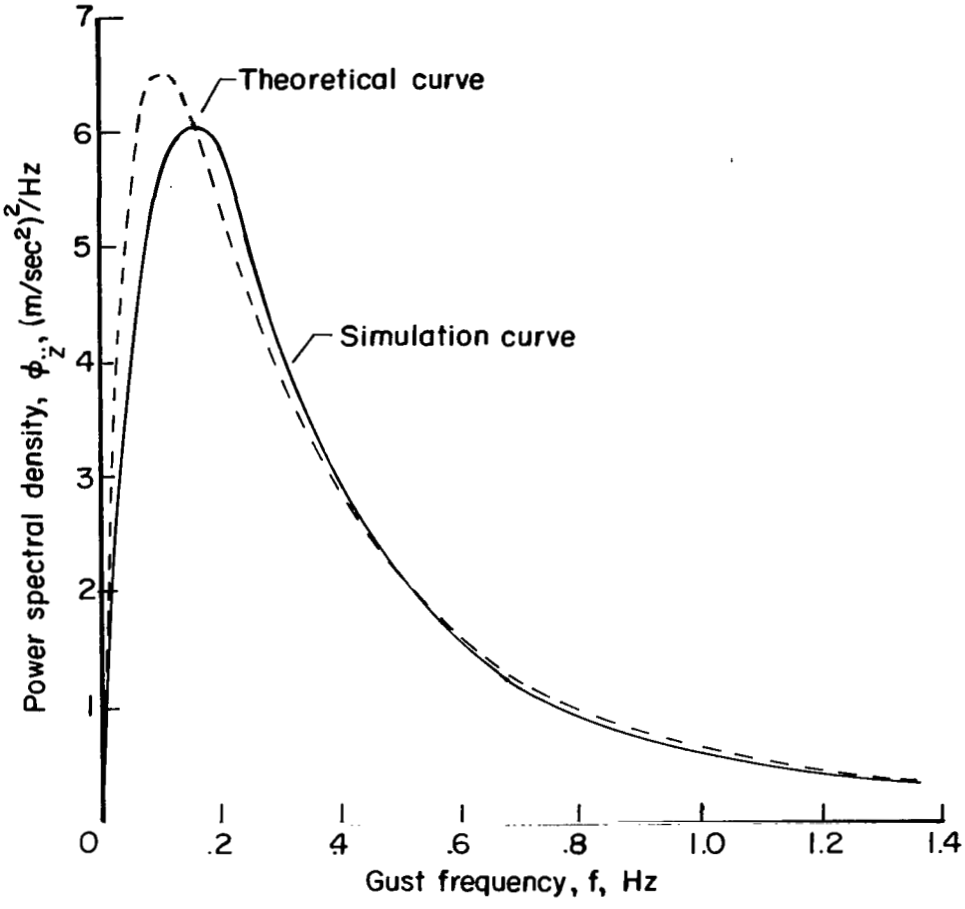

Figure 1.- Power spectral density of the vertical acceleration response to vertical gusts for the basic airplane (without alleviation). $\overline{w_g^2} = 9.3\ (m/sec)^2$; L = 610 m.

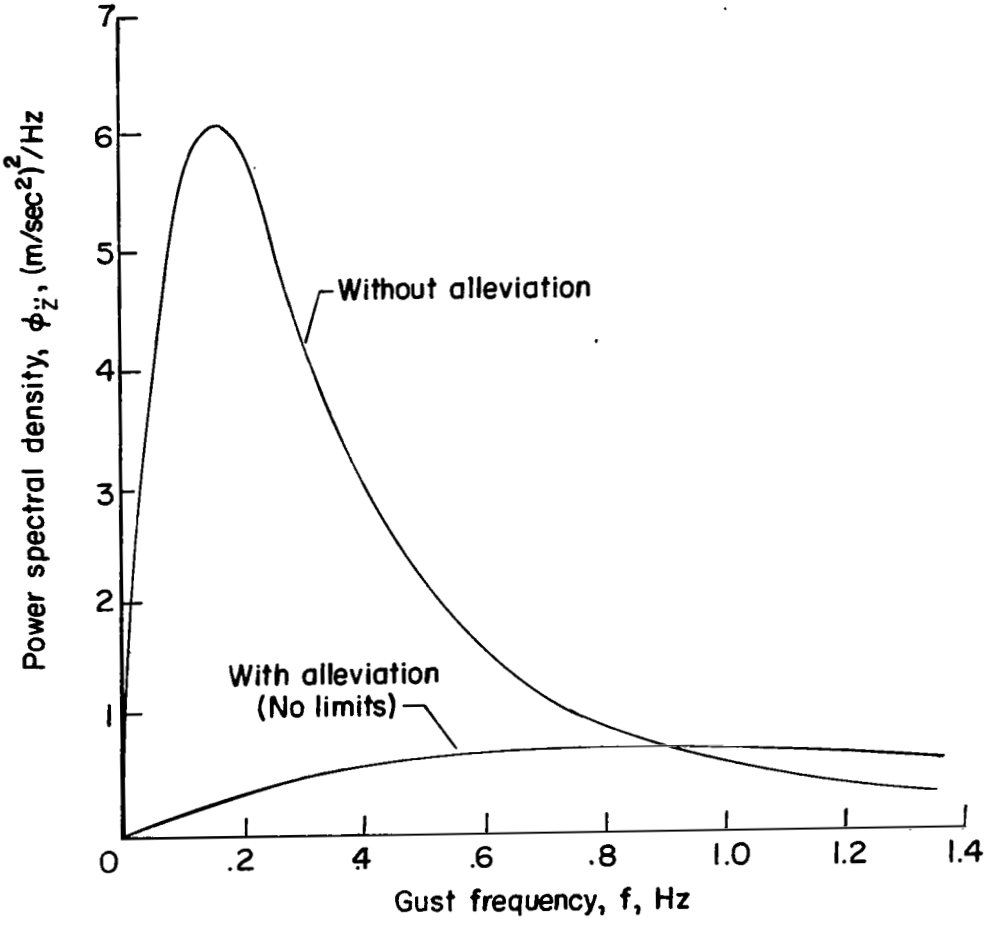

(a) Gust sensor located at wing aerodynamic center. $V_T = 0$.

Figure 2.- Effectiveness of alleviation system with no limits on flap motion. $\omega_n = 10$ rad/sec.

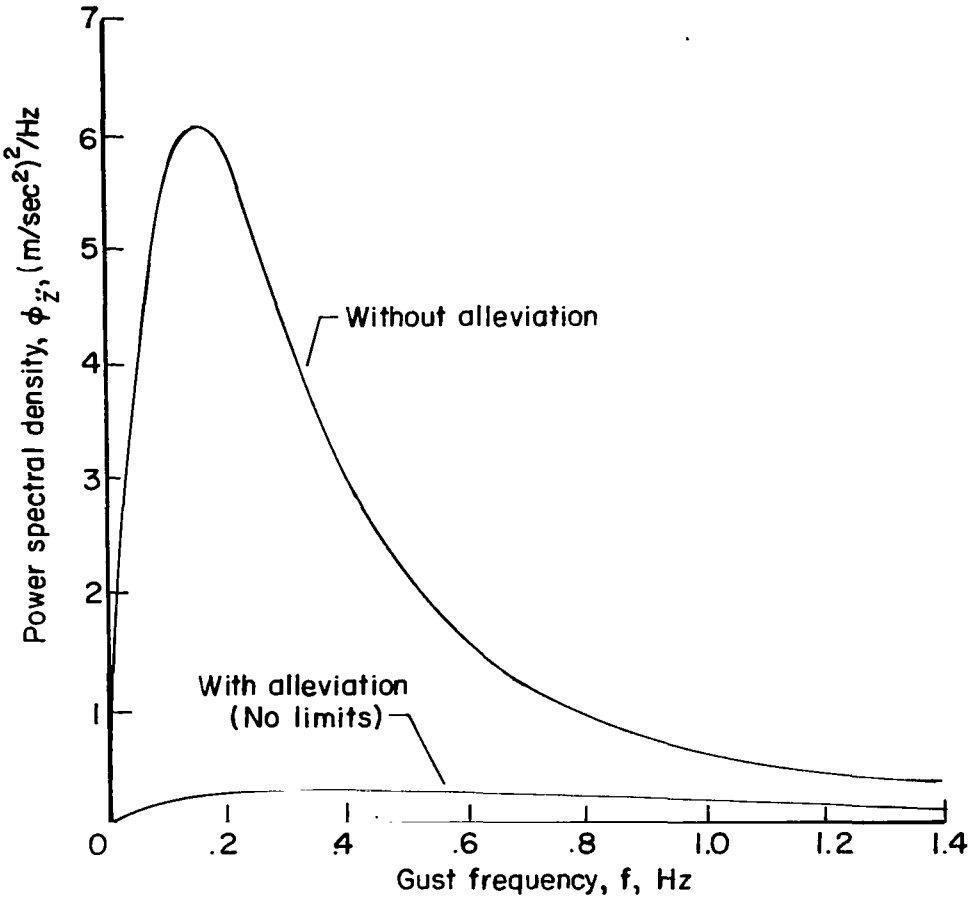

(b) Gust sensor located at $V\tau$ = 5.22 meters.

Figure 2.- Concluded.

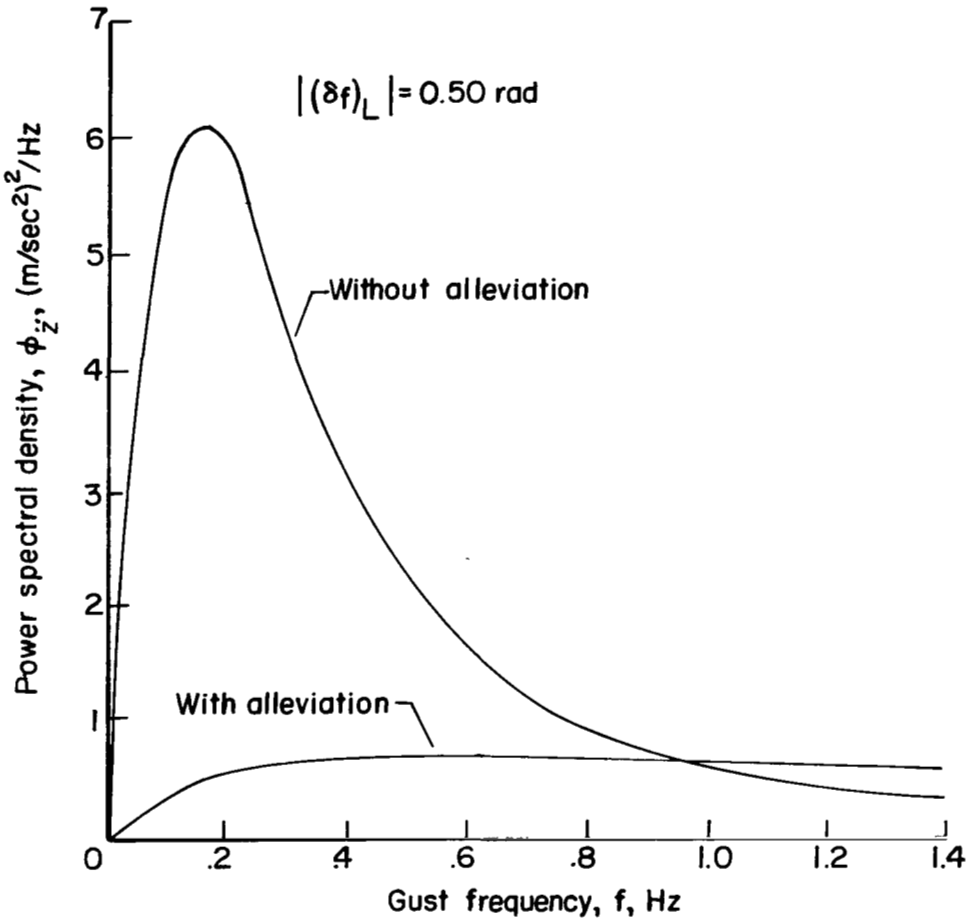

(a) Gust sensor located at wing aerodynamic center. $V\tau = 0$.

Figure 3.- Effectiveness of alleviation system with limits on amplitude of flap motion. $\omega_n = 10$ rad/sec.

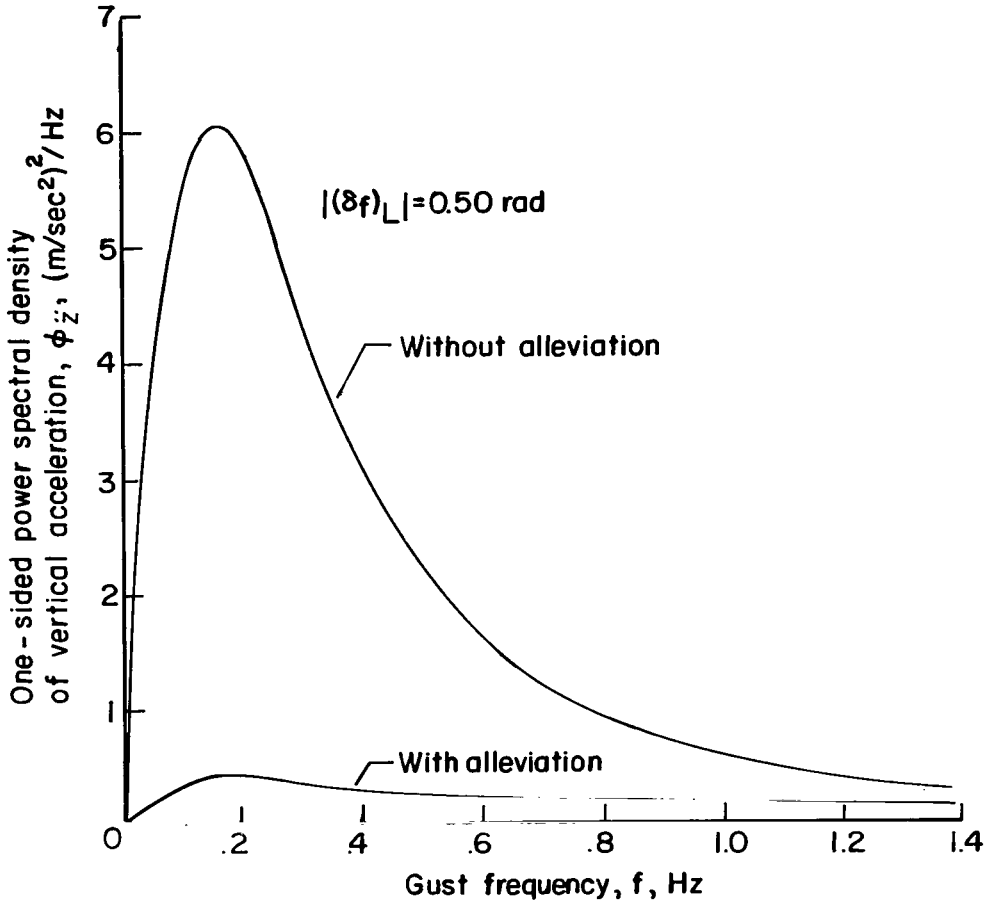

(b) Gust sensor located at V_T = 5.22 meters.

Figure 3.- Concluded.

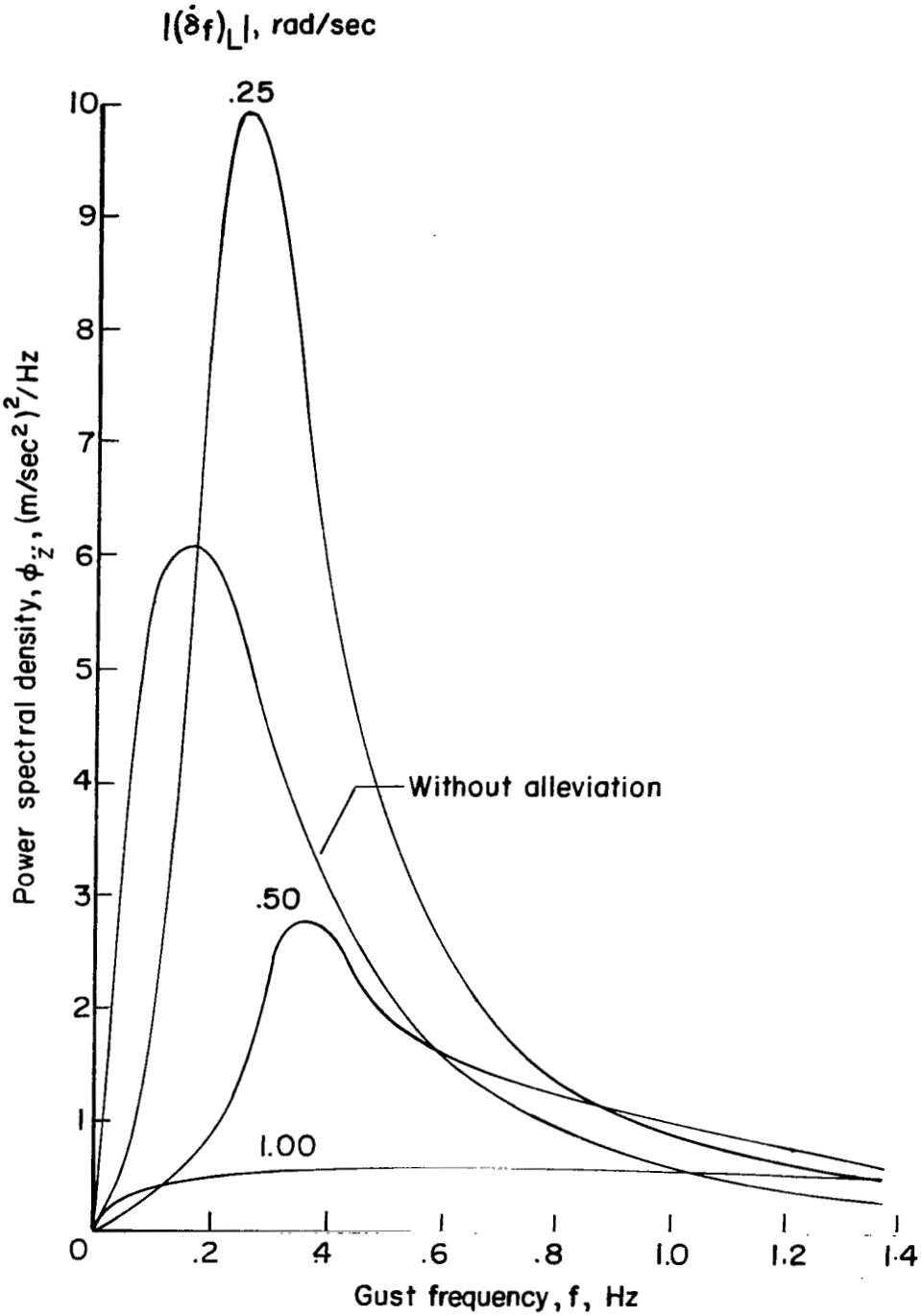

(a) Gust sensor located at wing aerodynamic center. $V_T = 0$.

Figure 4.- Effectiveness of alleviation system with limits on rate of flap motion. $\omega_n = 10$ rad/sec; $\left|(\delta_f)_L\right| = 0.50$ rad.

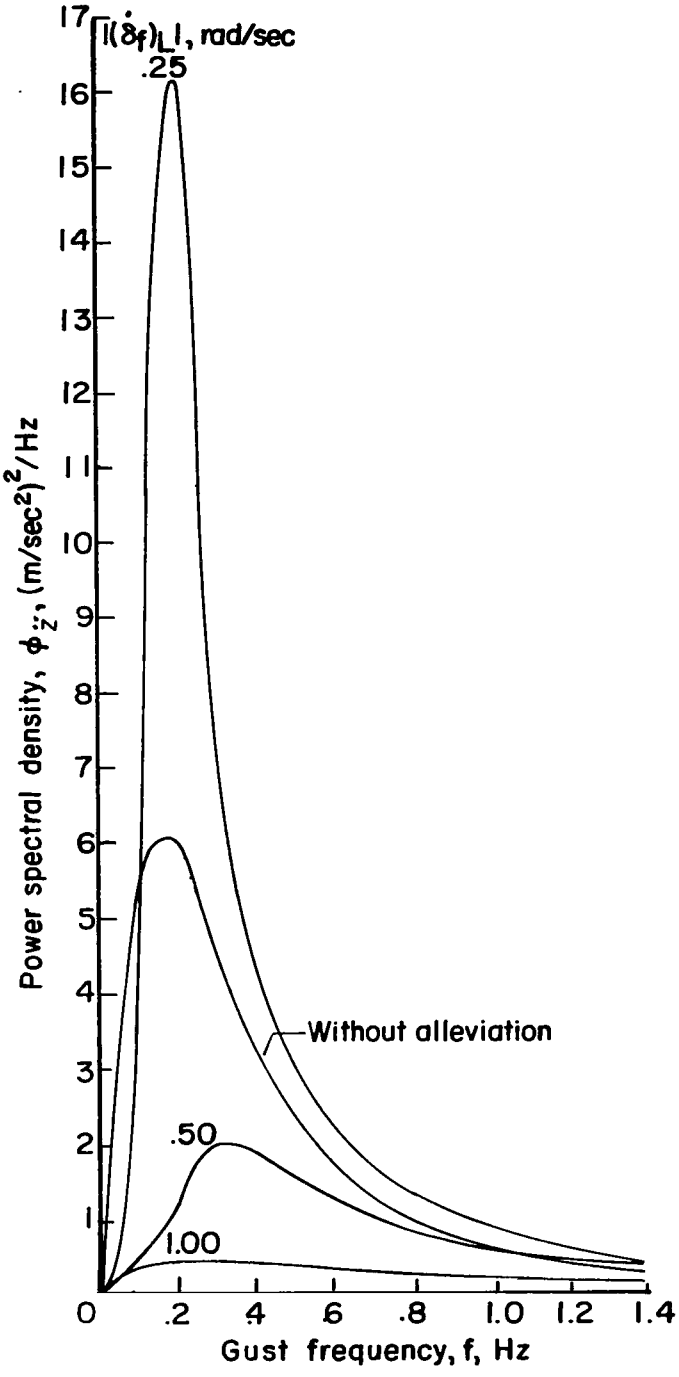

(b) Gust sensor located at $V\tau$ = 5.22 meters.

Figure 4.- Concluded.

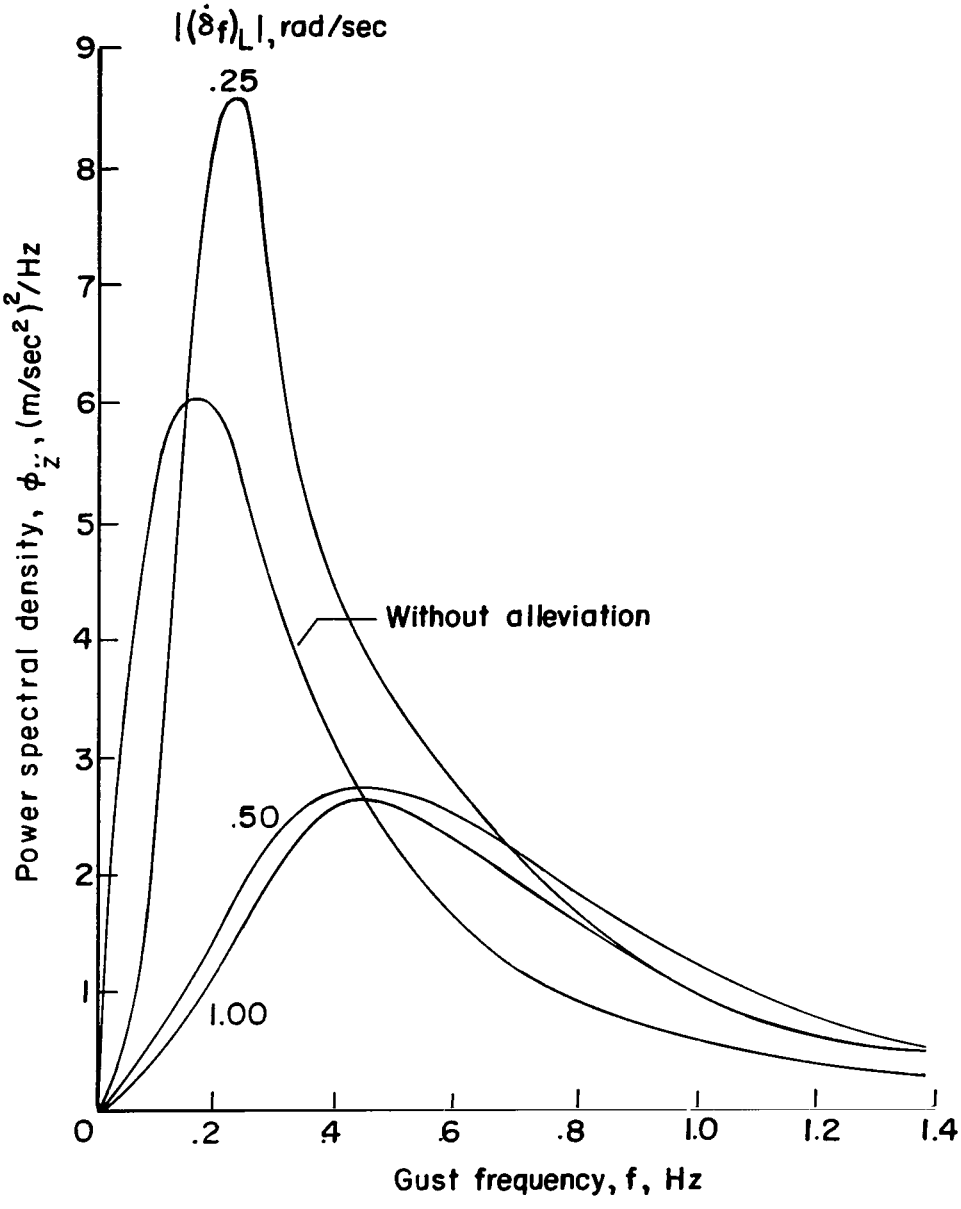

(a) Gust sensor located at wing aerodynamic center. $V_T = 0$.

Figure 5.- Effectiveness of alleviation system with limits on rate of flap motion. $\omega_n = 4$ rad/sec; $\left|(\delta_f)_L\right| = 0.50$ rad.

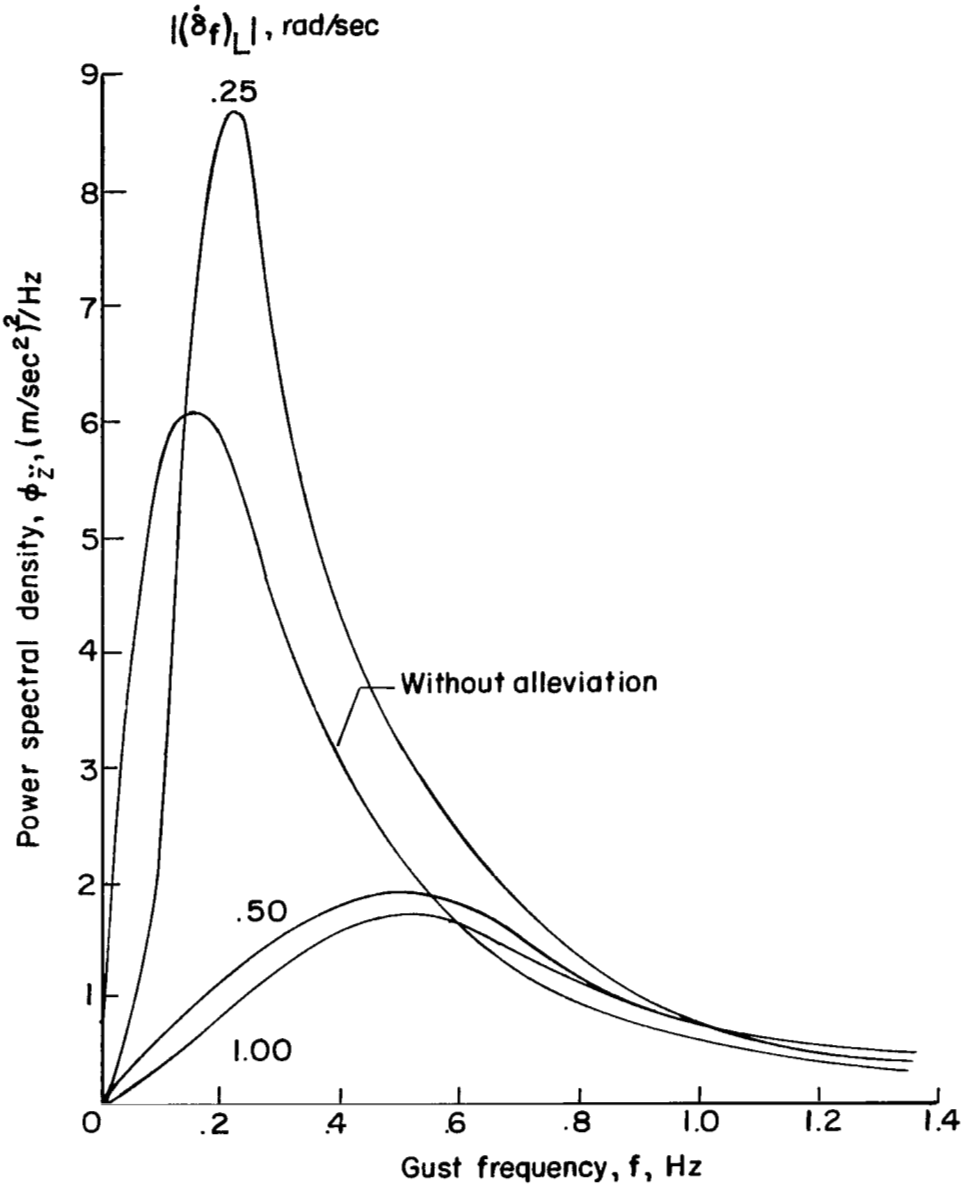

(b) Gust sensor located at V_T = 5.22 meters.

Figure 5.- Concluded.

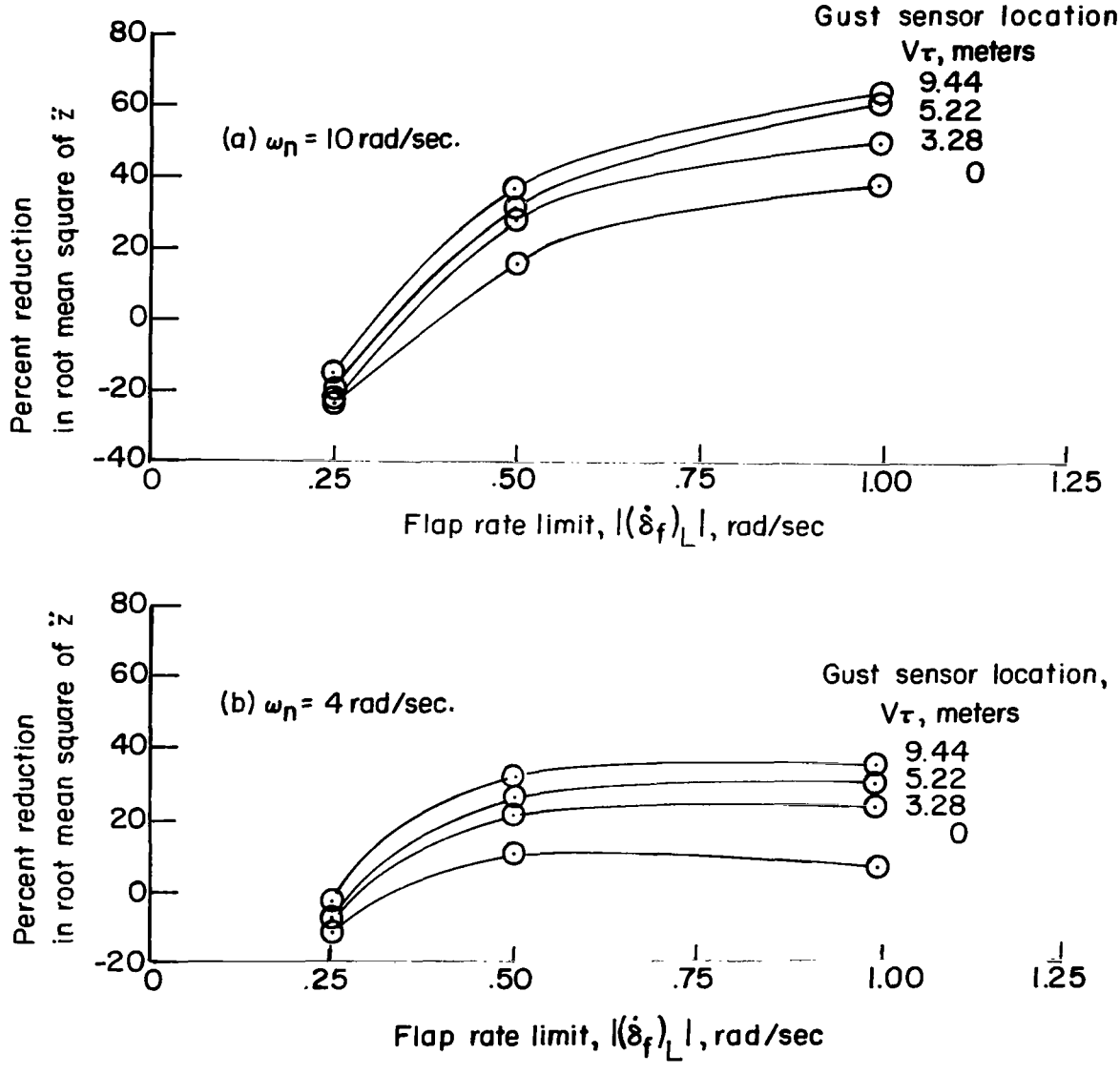

Figure 6.- Effect of flap rate limit on root mean square of vertical acceleration. $\left|(\delta f)_L\right| = 0.50$.

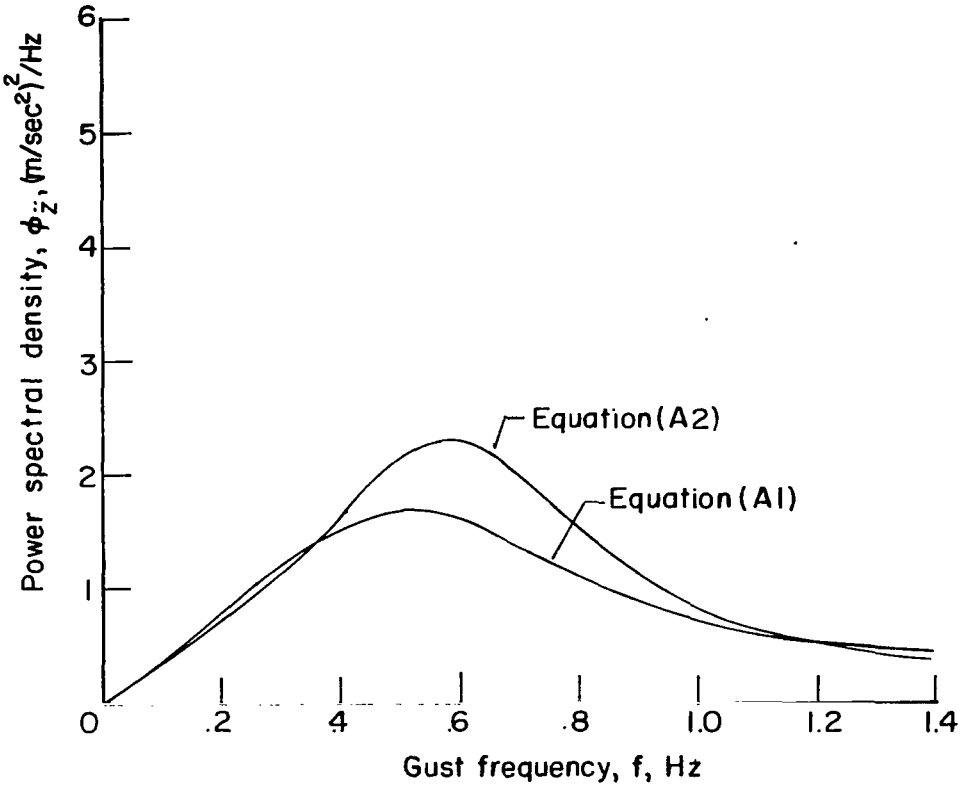

(a) $\left|\left(\dot{\delta}_f\right)_L\right|$ = 1.0 rad/sec.

Figure 7.- Power spectral density of vertical acceleration resulting from the use of equations (A1) and (A2). ω_n = 4 rad/sec; V_T = 5.22 meters; $\left|\left(\delta_f\right)_L\right|$ = 0.5 rad.

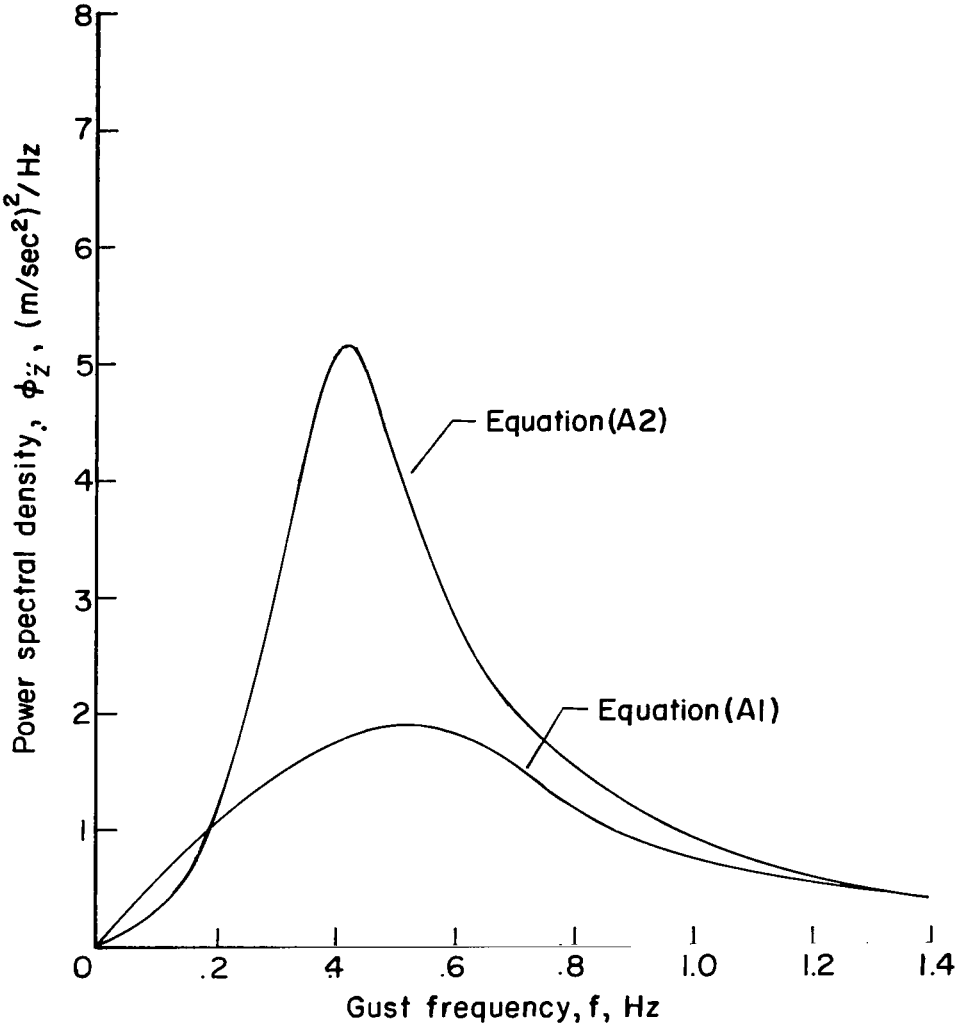

(b) $\left|\left(\dot{\delta}_f\right)_L\right|$ = 0.5 rad/sec.

Figure 7.- Continued.

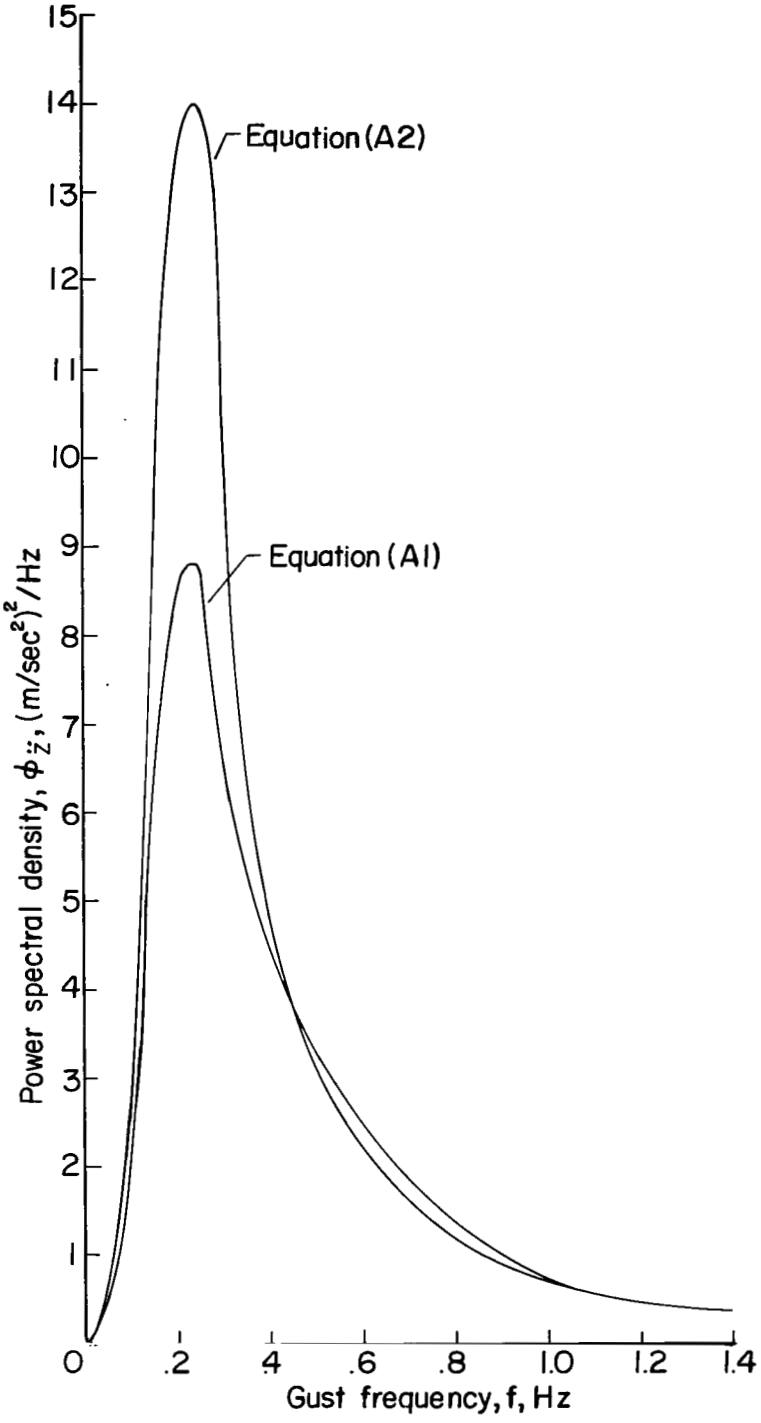

(c) $\left|\left(\dot{\delta}_f\right)_L\right|$ = 0.25 rad/sec.

Figure 7.- Concluded.

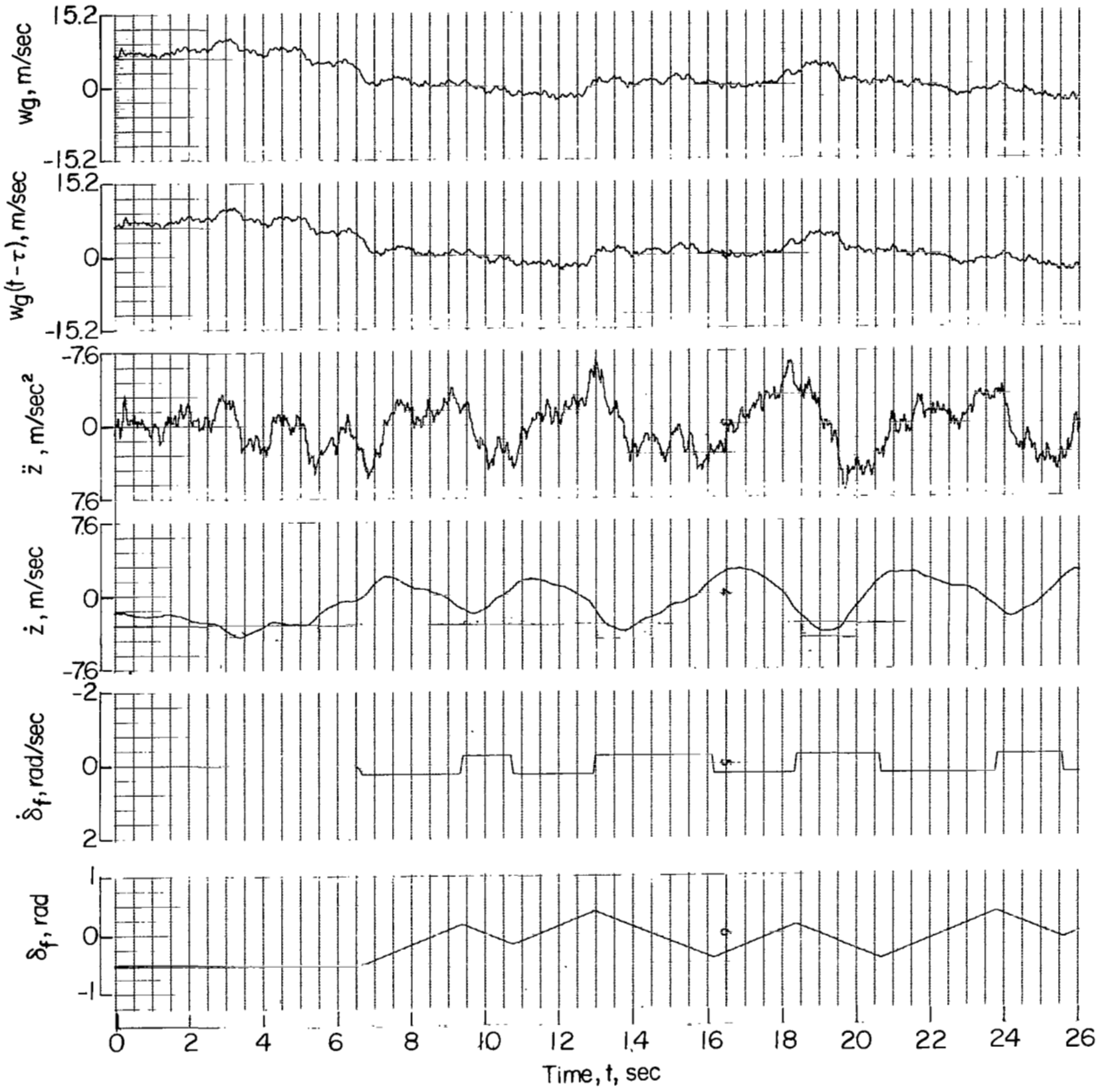

Figure 8.- Time histories illustrating limit-cycle oscillations which can result with flap limit and velocity feedback control. ω_n = 4 rad/sec; $\left|(\delta_f)_L\right|$ = 0.5 rad; $\left|(\dot{\delta}_f)_L\right|$ = 0.25 rad/sec.

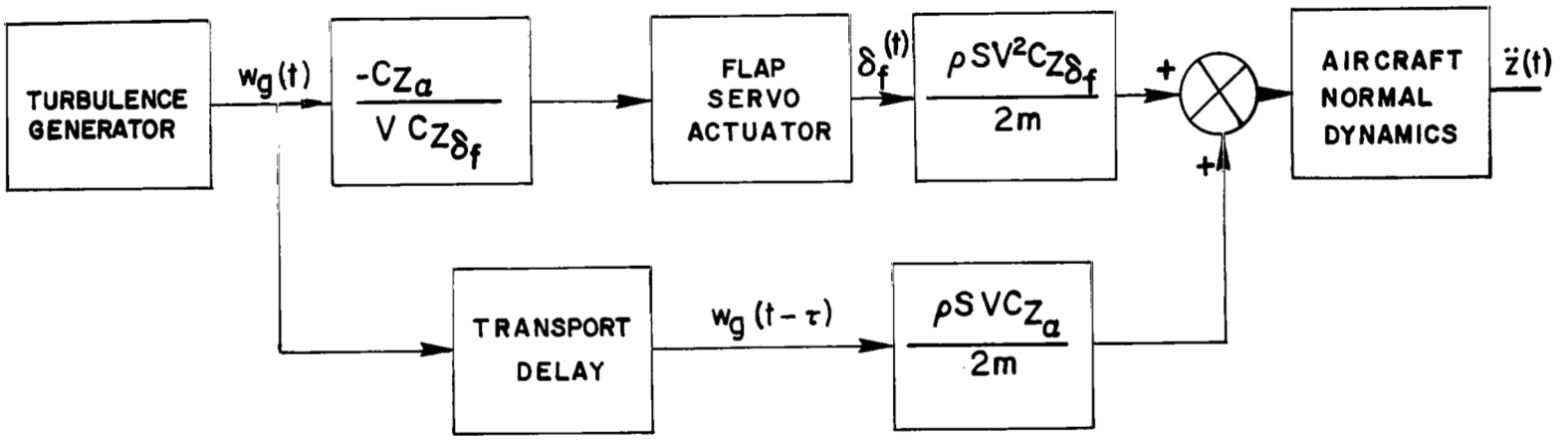

Figure 9.- Simulation of gust-alleviation system.

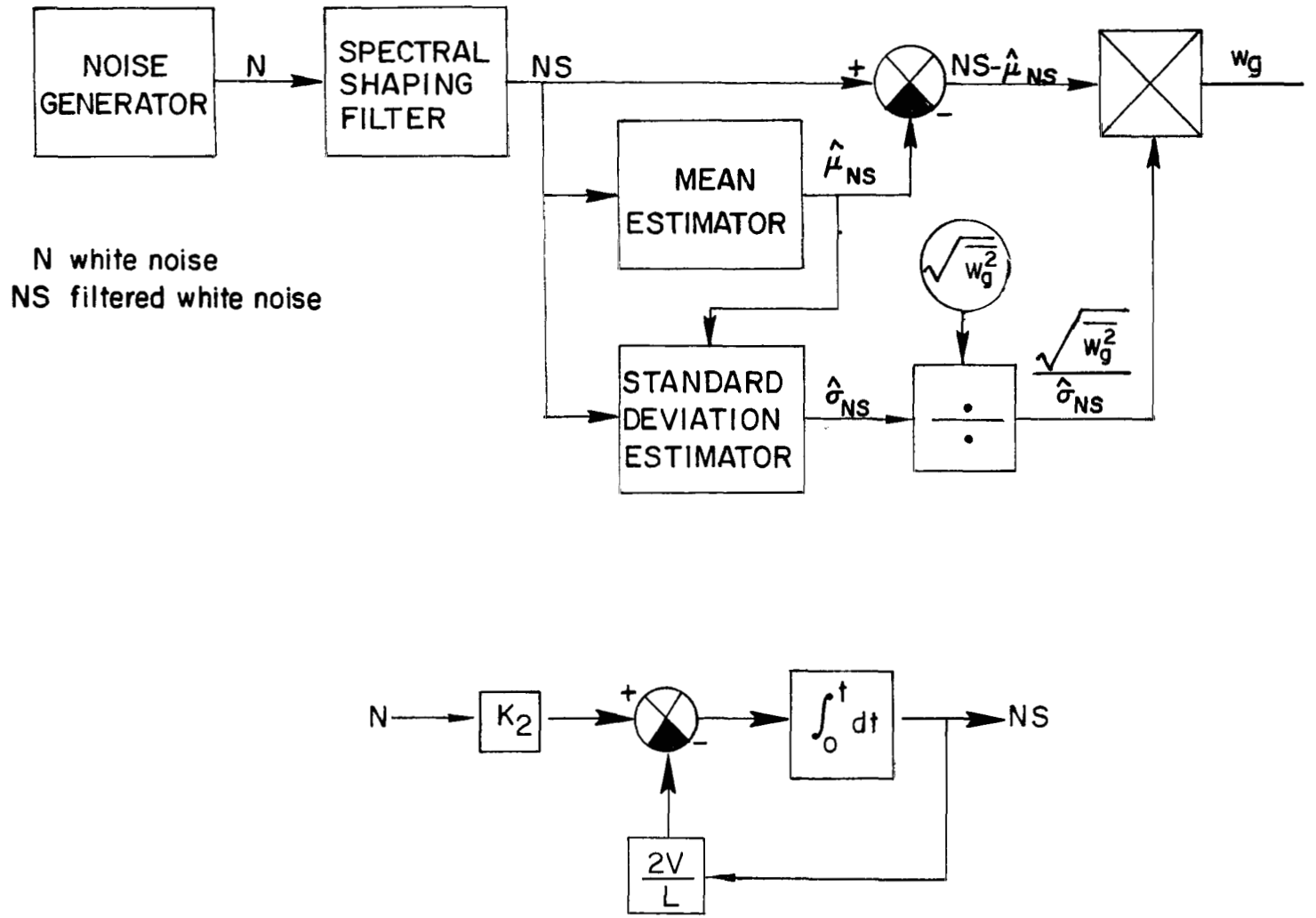

Figure 10.- Turbulence generator.

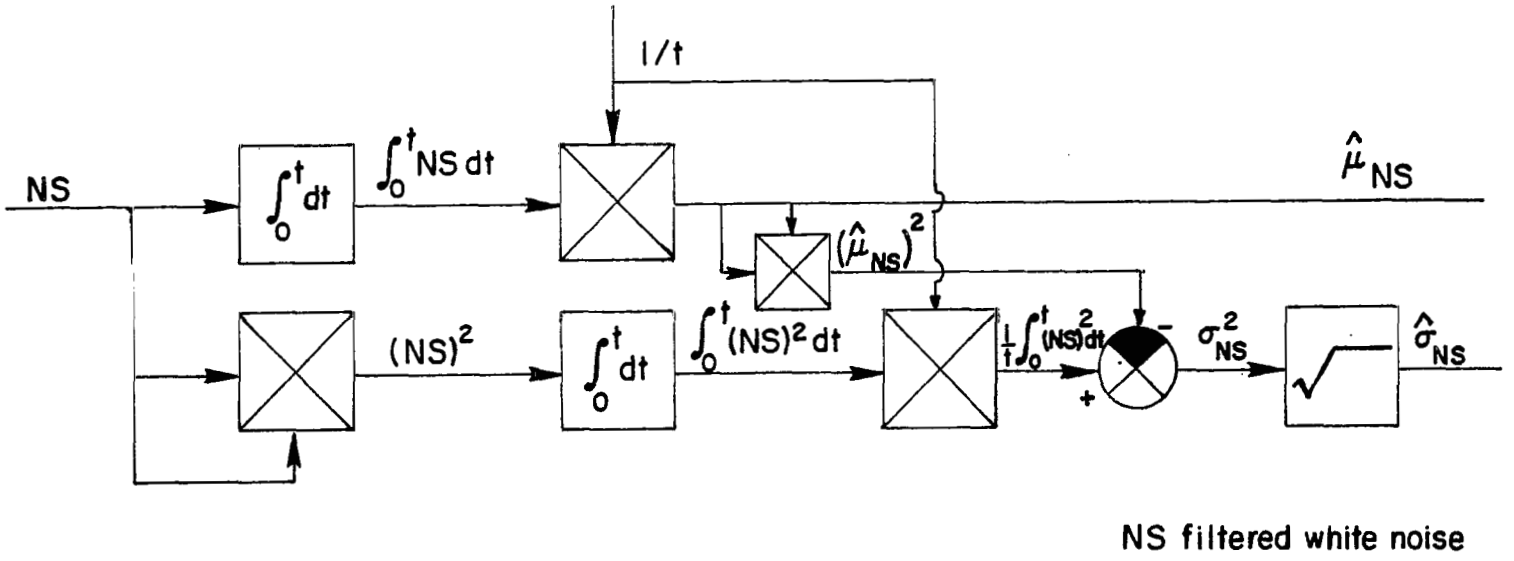

Figure 11.- Estimation of mean and standard deviation.

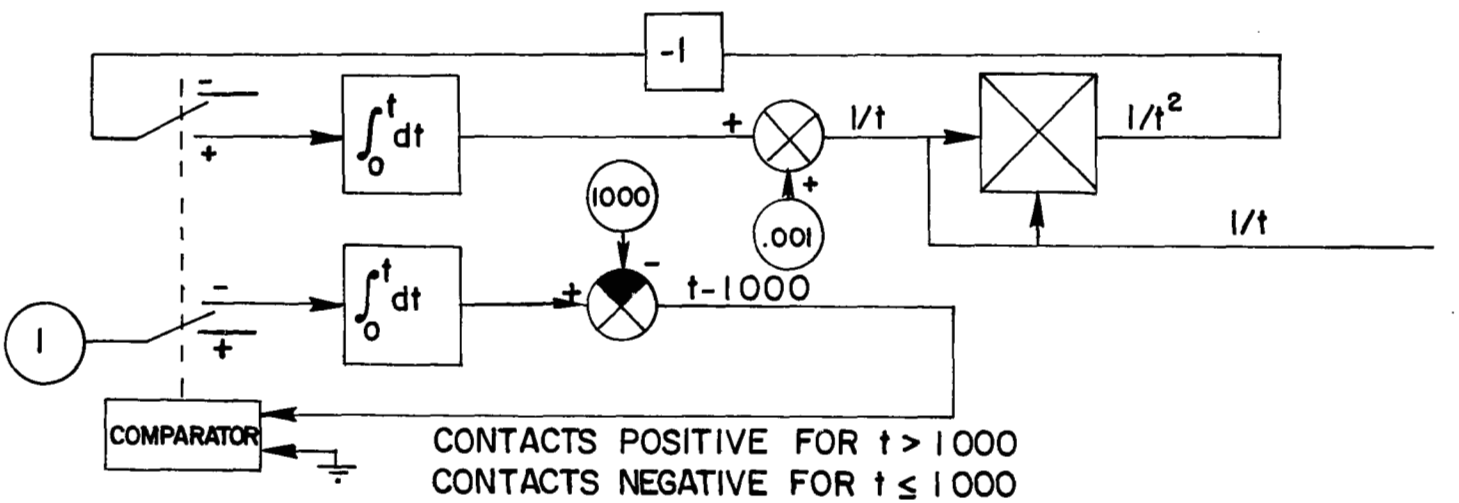

Figure 12.- Generation of (1/t) for $t \geq 1000$ seconds.

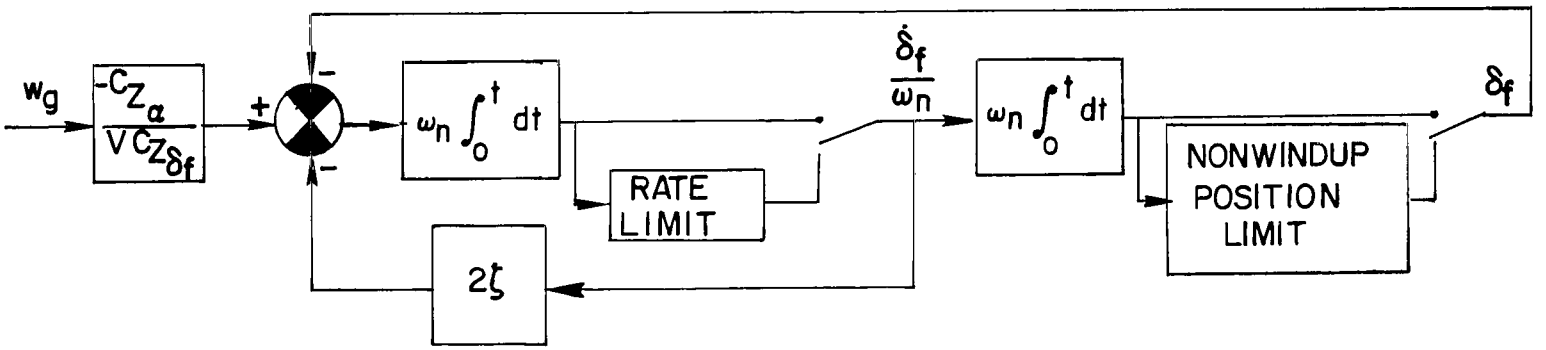

Figure 13.- Flap with selectable limits.

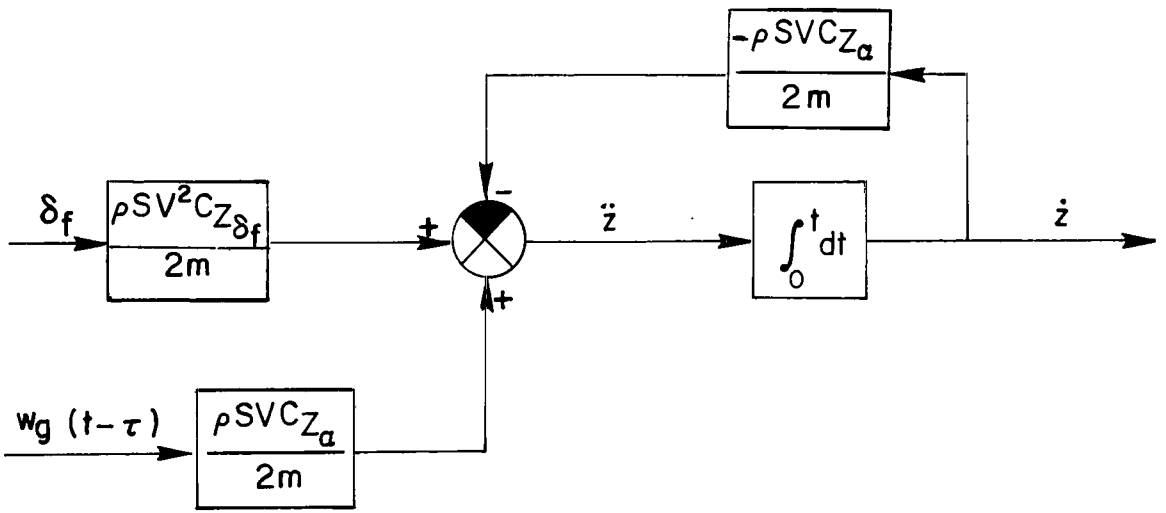

Figure 14.- Aircraft dynamics.

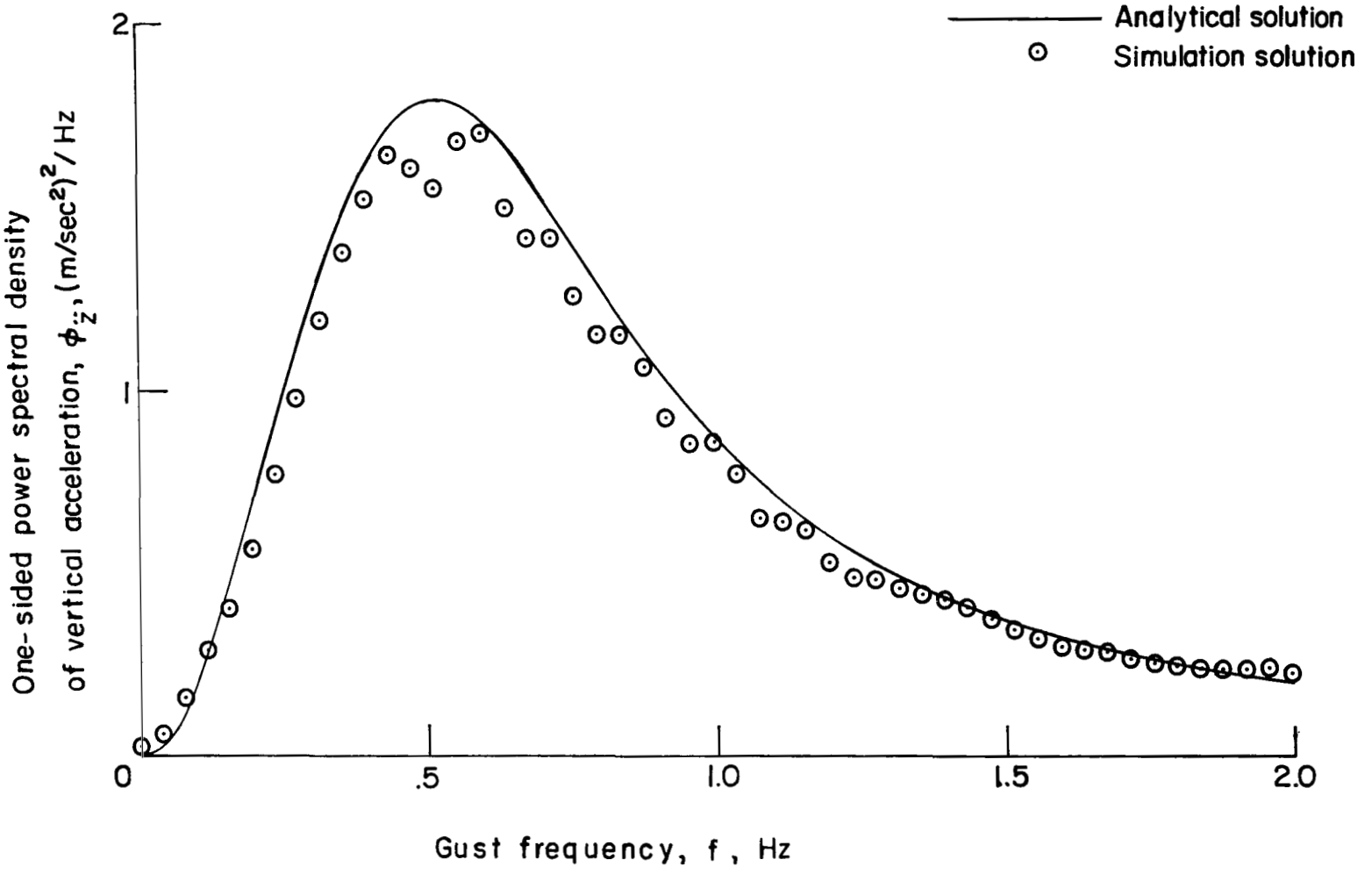

Figure 15.- Comparison of analytical and simulation solutions (no limits). $\omega_n = 4$ rad/sec; $\zeta = 0.7$; $\tau = 0.078$ sec.

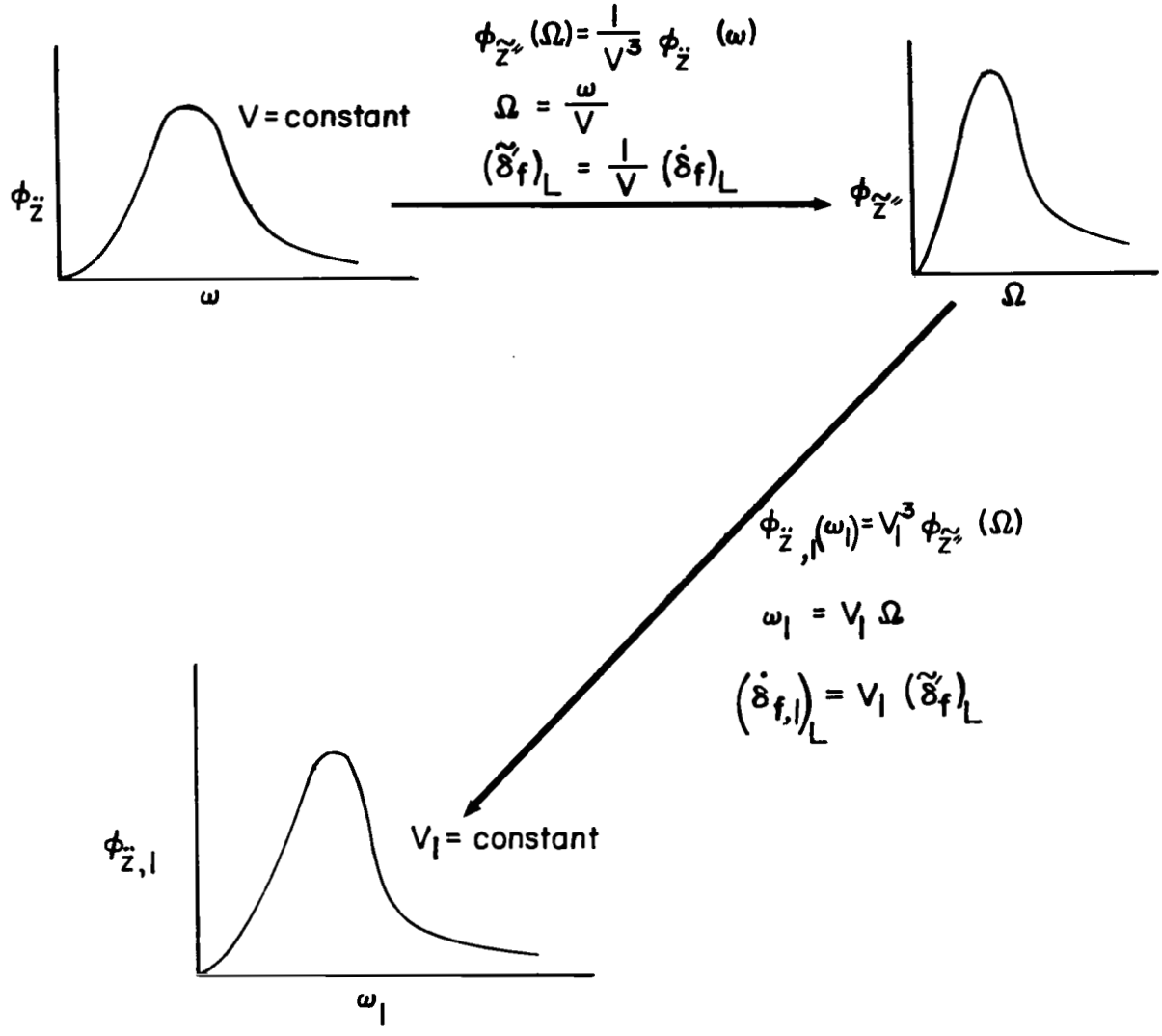

Figure 16.- Relationships between power spectral densities when gust intensity varies with velocity and ζ, $V\tau$, ω_n/V, and $(\delta_f)_L$ are held constant.

"The aeronautical and space activities of the United States shall be conducted so as to contribute . . . to the expansion of human knowledge of phenomena in the atmosphere and space. The Administration shall provide for the widest practicable and appropriate dissemination of information concerning its activities and the results thereof."

— NATIONAL AERONAUTICS AND SPACE ACT OF 1958

NASA SCIENTIFIC AND TECHNICAL PUBLICATIONS

TECHNICAL REPORTS: Scientific and technical information considered important, complete, and a lasting contribution to existing knowledge.

TECHNICAL NOTES: Information less broad in scope but nevertheless of importance as a contribution to existing knowledge.

TECHNICAL MEMORANDUMS: Information receiving limited distribution because of preliminary data, security classification, or other reasons.

CONTRACTOR REPORTS: Scientific and technical information generated under a NASA contract or grant and considered an important contribution to existing knowledge.

TECHNICAL TRANSLATIONS: Information published in a foreign language considered to merit NASA distribution in English.

SPECIAL PUBLICATIONS: Information derived from or of value to NASA activities. Publications include conference proceedings, monographs, data compilations, handbooks, sourcebooks, and special bibliographies.

TECHNOLOGY UTILIZATION PUBLICATIONS: Information on technology used by NASA that may be of particular interest in commercial and other non-aerospace applications. Publications include Tech Briefs, Technology Utilization Reports and Technology Surveys.

Details on the availability of these publications may be obtained from:

SCIENTIFIC AND TECHNICAL INFORMATION OFFICE

NATIONAL AERONAUTICS AND SPACE ADMINISTRATION

Washington, D.C. 20546